Computers and Fluids 197 (2020) 104374

Contents lists available at ScienceDirect

Computers and Fluids

journal homepage: www.elsevier.com/locate/compfluid

A fractional step method for computational aeroacoustics using weak imposition of Dirichlet boundary conditions

Samuel Parada [a], Joan Baiges [a,*], Ramon Codina [a,b]

[a] Universitat Politècnica de Catalunya, Barcelona Tech, Jordi Girona 1-3, Edifici C1, 08034 Barcelona, Spain
[b] Centre Internacional de Mètodes Numèrics en Enginyeria (CIMNE), Edifici C1, Campus Nord UPC, Gran Capità s/n, 08034 Barcelona, Spain

ARTICLE INFO

Article history:
Received 23 May 2019
Revised 29 October 2019
Accepted 7 November 2019
Available online 12 November 2019

Keywords:
Isentropic flow
Fractional step methods
Weak boundary conditions
Term-by-term stabilization
Aeroacoustics

ABSTRACT

In this work we consider the approximation of the isentropic Navier–Stokes equations. The model we present is capable of taking into account acoustic and flow scales at once. After space and time discretizations have been chosen, it is very convenient from the computational point of view to design fractional step schemes in time so as to permit a segregated calculation of the problem unknowns. While these segregation schemes are well established for incompressible flows, much less is known in the case of isentropic flows. We discuss this issue in this article and, furthermore, we study the way to weakly impose Dirichlet boundary conditions via Nitsche's method. In order to avoid spurious reflections of the acoustic waves, Nitsche's method is combined with a non-reflecting boundary condition. Employing a purely algebraic approach to discuss the problem, some of the boundary contributions are treated explicitly and we explain how these are included in the different steps of the final algorithm. Numerical evidence shows that this explicit treatment does not have a significant impact on the convergence rate of the resulting time integration scheme. The equations of the formulation are solved using a subgrid scale technique based on a term-by-term stabilization.

1. Introduction

Within the field of Computational Aeroacoustics (CAA), the solution of the complete set of Navier–Stokes equations written in its conservative form, i.e., the coupled problem involving mass, momentum and energy conservation equations, is referred as Direct Noise Computation (DNC) [1]. This formulation represents a direct path to consistently deal with aerodynamic and acoustic scales in an unified manner. The solution of this fully compressible problem via the Finite Element Method (FEM) [2] is known to be excessively demanding in terms of computational power. Likewise, most of the compressible flow solvers found in the literature exhibit an inadequate performance in the low Mach number regime. This is mainly due to the fact that flow and acoustic scales start to considerably differ one from each other under the subsonic condition as the Mach number is progressively reduced. As a consequence, the algebraic systems arising from those formulations are usually ill-conditioned.

With the aim of overcoming such conditioning issues, several hybrid methods arose for which the computations of aerodynamics and acoustics are decoupled and hence solved independently. The most remarkable work in this area is probably the well-known Lighthill analogy [3], in which the acoustic field is obtained upon the derivation of a source term computed with the flow equations. It is also worth mentioning the socalled incompressible-acoustic split method (see e.g. [4–6] and references therein) which consists in solving the incompressible Navier–Stokes equations followed by an inviscid acoustic part which accounts for the wave propagation. In [7], this approach is revised by also retaining the viscous terms in the acoustic set of equations. The advantage of these techniques with respect to the acoustic analogies is that the source term is directly obtained and it accounts for both sound generation and scattering. These type of hybrid methods allow a certain flexibility, in the sense that they permit the usage of different models for flow and acoustics. However, since the incompressible problem is solved prior to the acoustic one, these methods do not account for feedback from acoustics to the flow.

The methodology used in this work aims at combining the simplicity of hybrid methods with the unified scale computation of DNC. Assuming a low Mach number flow with neither shocks nor thermal sources, and entropy to remain constant, a simplified compressible Navier–Stokes problem involving only velocity and

* Corresponding author.
E-mail addresses: samuel.parada@upc.edu (S. Parada), joan.baiges@upc.edu (J. Baiges), ramon.codina@upc.edu (R. Codina).

https://doi.org/10.1016/j.compfluid.2019.104374
0045-7930/

pressure fields as unknowns can be derived. This is the socalled isentropic flow problem [8]. Solving monolithically the algebraic system of equations that arises after the discretization via the finite element method of the continuous isentropic problem is the classical solution strategy. Despite of the several simplifications that can be introduced thanks to the constant entropy assumption, solving the resulting linear system of equations might still be computationally expensive, specially in 3D geometries. The unknowns are highly coupled and nonlinearities need to be solved too. An alternative to that standard approach is to solve the problem by means of a fractional step method in time. This technique consists in segregating the calculation of the unknowns, so that they can be computed separately, probably with the addition of some correction steps. On the negative side, fractional step methods have an associated temporal error, frequently labeled as fractional or segregation error. It is indispensable to ensure that such error is at least of the order of the integration scheme used in time, with the purpose of maintaining the global temporal accuracy of the method.

Fractional step methods were originally called *projection methods* (indistinctly called fractional step or segregation methods in the following) as they were based on the decomposition of differential operators at the continuous level. The pioneering works of Chorin and Temam [9,10] in the late1960/s established the basis of this novel technique. Apart from this continuous approach, fractional step methods can be introduced at the purely algebraic level too. For a review on both approaches in the case of the incompressible Navier–Stokes equations, we refer the reader to [11,12]. Eventually, fractional step methods have enjoyed an extensive recognition mainly due to two reasons: they allow an important reduction of computational time and present an intrinsic stability over the pressure gradient term [13].

Apart from a possible compatibility restriction between velocity and pressure interpolating spaces, the convective terms appearing in the governing equations may render the solution unstable when using a finite element formulation, showing spurious node-to-node oscillations. Though this fluctuating behavior could be avoided setting a specific mesh size (which commonly is not computationally affordable), stabilized formulations appear to circumvent this issue. In these formulations, the weak form of the problem obtained by the classical Galerkin method is modified upon the introduction of some mesh-dependent terms weighted by the residuals (or even part of them) of the differential equations. Several numerical techniques have been developed within this context: the well known Streamline/Upwind-Petrov-Galerkin (SUPG) method [14] or Galerkin-Least Square (GLS) method [15], the Taylor-Galerkin method [16] and the Variational Multi-Scale method (VMS) [17,18], being the latter the one adopted in this work. The VMS technique provides a general variational framework for subgrid scale models [19].

The key idea behind the VMS approach is to split the unknowns of the problem into two scales, namely, the scale that can be approximated by the finite element mesh and the subgrid scale, the unresolvable one. The general methodology consists in finding an approximation for the subgrid scale so as to yield a stable formulation involving only the finite element scales, hence maintaining the number of degrees of freedom of the starting Galerkin variational problem. There are different ways to model the subgrid scale, provided a definition of the functional space where it belongs. In this article, we will define such space as the orthogonal one to the finite element space and, using this concept, we will state a term-by-term technique by neglecting the extra cross products which do not play any stability role in the formulation. As a result, this stabilized formulation is not residual based, and hence not consistent, being consistency understood in the classical finite element context. However, for the incompressible flow problem this term-by-term possibility provides a slightly improved pressure stability [20], and in [21,22] it was applied to the viscoelastic flow problem making it possible to solve more elastic cases than a residual-based formulation.

Another important feature of nearly incompressible aeroacoustic flows is that external computational boundaries may produce deceptive wave reflections which pollute the solution. Ingoing waves can interfere with acoustic signals as well as originate numerical instabilities if the numerical technique is unable to introduce enough dissipation. This distinguishing issue has been widely studied and as a result, there are several numerical techniques which deal with the backscattering of waves in the field of aeroacoustics. Among the most remarkable ones are: the damping of the compressible equations, the addition of an artificial counter signal, and the application of non-reflecting boundary conditions. Performing a damping of some terms of the compressible equations is a robust approach to face spurious reflections at the boundary (buffer zones). However, this technique brings an extra computational effort associated with the new terms that need to be included, and hence other approaches are often adopted. The literature on compressible boundary conditions is extensive, so we refer to the reviews in [23–25] and references therein. For the specific case of the isentropic problem, a novel method for the unified prescription of boundary conditions was introduced in [8] (Section 3). The particularity of the method is that it combines a weak imposition of Dirichlet boundary conditions [26] of the mean flow variables, plus a Sommerfeld non-reflecting boundary condition for the acoustic component of the pressure [27].

In this paper, we present an algrebraic-fractional step method in time which allows to solve the isentropic Navier–Stokes problem in a segregated manner. Our algorithm includes a stabilization within the VMS framework, making use of the orthogonal subscale concept to derive a term-by-term technique. In order to avoid any artificial reflection at the external boundaries, we incorporate the above-mentioned unified prescription of boundary conditions for the isentropic problem, formulating here its segregated counterpart. The set of equations to be discussed in the following can be understood as an extension of the incompressible case, since the final problem to be solved requires to compute only velocity and pressure fields, being the thermal problem mathematically uncoupled. This is possible due to the constant entropy assumption, which in turn allows to a establish a direct connection between density and pressure derivatives. As a result, the isentropic model presents two main advantages: first it takes into account any possible acoustic feedback on the flow scales and second, the validity of the acoustic field is not subjected to the particular motion of the flow. On top of that, the computational cost of the present technique is reduced with respect to other methods. Apart from the fact that both acoustic and flow scales are solved altogether and that we get rid of the energy conservation equation, the final system is better conditioned (we refer to [8] for a detailed discussion on this).

The article is organized as follows: in Section 2 the isentropic compressible Navier–Stokes equations are introduced, as well as its variational formulation. The details of the compatible prescription of boundary conditions are reviewed in Section 3, whereas in Section 4 we present the variational formulation and the monolithic time discretization of the problem with the boundary conditions described earlier. Section 5 is devoted to the design of the fractional step scheme from an algebraic viewpoint, taking into account the modifications due to the application of boundary conditions. In Section 6, we state the stabilized finite element formulation we favor, together with the relevant adjustments that need to be considered. Numerical experiments are conducted in Section 7 and, finally, conclusions are drawn in Section 8.

2. Isentropic compressible flow problem

2.1. Initial considerations

Let us start the exposition of our work by recalling some of the basic relations of the compressible flow theory for ideal gases, (see e.g. [28] for details). By definition of an isentropic flow, the entropy remains constant. This fact allows one to show that pressure and density are related through the following fundamental expression,

$$\frac{p}{\varrho^\gamma} = \mathcal{C} \qquad \text{(a constant)}, \tag{1}$$

where γ is the socalled adiabatic coefficient, $\gamma \doteq c_p/c_v$, being c_p and c_v the specific heat of the fluid at constant pressure and volume, respectively. Additionally, p denotes the total pressure and ϱ is the total density, including any probable perturbations that the compressible nature of the medium might cause. There exist two useful expressions which relate density and pressure for two locations, being one of them at the stagnation conditions, that is to say, those that would exist if the flow at any point of a stream was isentropically brought to rest,

$$\frac{\varrho_0}{\varrho} = \left(1 + \frac{\gamma-1}{2}\mathrm{Ma}^2\right)^{\frac{1}{\gamma-1}}, \tag{2}$$

$$\frac{p_0}{p} = \left(1 + \frac{\gamma-1}{2}\mathrm{Ma}^2\right)^{\frac{\gamma}{\gamma-1}}, \tag{3}$$

where $(\cdot)_0$ stands for variables at stagnation conditions. The symbol Ma refers to the Mach number, defined as $\mathrm{Ma} \doteq |\boldsymbol{u}|/c_0$ being $|\boldsymbol{u}|$ the modulus of the pointwise flow velocity and c_0 the speed of sound of an ideal gas, computed as $c_0 \doteq \sqrt{\gamma R\theta_0/M}$. In this last expression, R [J/K-mol] is the universal gas constant, M [kg/mol] is the molar mass of the gas under consideration and θ_0 [K] denotes the temperature.

Relating (2)-(3) one can easily derive the following equality,

$$\frac{p_0}{p} = \left(\frac{\varrho_0}{\varrho}\right)^\gamma, \tag{4}$$

which is in direct agreement with the fundamental expression of isentropic flows (1).

Now, taking derivatives with respect to time in both sides of (4) and recalling the equation of state of an ideal gas, i.e., $p_0 M = \varrho_0 R\theta_0$, an expression directly relating density and pressure time derivatives arises,

$$\partial_t p = \frac{p_0}{\varrho_0}\gamma\left(1 + \frac{\gamma-1}{2}\mathrm{Ma}^2\right)^{-1}\partial_t\varrho = \frac{R\theta_0}{M}\gamma\left(1 + \frac{\gamma-1}{2}\mathrm{Ma}^2\right)^{-1}\partial_t\varrho,$$

where the standard short notation for the time derivative was introduced. If instead of the time derivative, one takes spatial derivatives, an equivalent expression can be found relating gradients. Both equations can be simplified if we identify the speed of sound as,

$$c = c_0\left(1 + \frac{\gamma-1}{2}\mathrm{Ma}^2\right)^{-\frac{1}{2}}, \tag{5}$$

so that in practice the following relations can be used,

$$\partial_t p = c^2\partial_t\varrho, \quad \nabla p = c^2\nabla\varrho. \tag{6}$$

Eq. (6) establishes a connection between pressure and density variations in a straightforward manner and it reduces the general complexity of the problem while making possible to capture the acoustic scales of the flow. This fact is in contraposition to other non-isentropic formulations for low Mach flows (see e.g. [29]) in which density variations might be related to temperature instead of pressure, and hence no acoustics are modeled.

2.2. Initial and boundary value problem

Let $\Omega \subset \mathbb{R}^d$ ($d = 2$ or 3) be a domain where we want to solve the isentropic Navier–Stokes problem during the time interval $[0, T]$. Considering a Newtonian fluid under isentropic compressible conditions, the system of partial differential equations is initially written as,

$$\begin{aligned} \varrho\partial_t\boldsymbol{u} + \varrho(\boldsymbol{u}\cdot\nabla)\boldsymbol{u} - \mu\Delta\boldsymbol{u} - \frac{\mu}{3}\nabla(\nabla\cdot\boldsymbol{u}) + \nabla p = \boldsymbol{f} \quad &\text{in } \Omega\times(0,T), \\ \partial_t\varrho + (\boldsymbol{u}\cdot\nabla)\varrho + \varrho\nabla\cdot\boldsymbol{u} = 0 \quad &\text{in } \Omega\times(0,T), \end{aligned}$$

where ϱ is the density, p is the pressure, $\boldsymbol{u}$ stands for the velocity field, μ for the fluid dynamic viscosity, and $\boldsymbol{f}$ is a given force vector. As usual, bold characters refer to vector variables and the symbol $\Delta(\cdot)$ denotes the Laplacian operator. Making use of (6), the continuity equation can be reformulated so that density derivatives are replaced by pressure derivatives. Hence, the problem finally consists in finding the fluid velocity $\boldsymbol{u} : \Omega\times(0,T) \to \mathbb{R}^d$ and the pressure $p : \Omega\times(0,T) \to \mathbb{R}$, which are solution of the following strong form of the isentropic compressible Navier–Stokes problem,

$$\varrho\partial_t\boldsymbol{u} + \varrho(\boldsymbol{u}\cdot\nabla)\boldsymbol{u} - \mu\Delta\boldsymbol{u} - \frac{\mu}{3}\nabla(\nabla\cdot\boldsymbol{u}) + \nabla p = \boldsymbol{f} \quad \text{in } \Omega\times(0,T), \tag{7}$$

$$\frac{1}{\varrho c^2}\partial_t p + \frac{1}{\varrho c^2}(\boldsymbol{u}\cdot\nabla)p + \nabla\cdot\boldsymbol{u} = 0 \quad \text{in } \Omega\times(0,T), \tag{8}$$

where the sound velocity c can be computed using (5). Problem (7) – (8) can be rewritten in a more compact manner. If we define $\boldsymbol{U} \doteq [\boldsymbol{u}, p]^\intercal$, $\boldsymbol{F} = [\boldsymbol{f}, 0]^\intercal$ and,

$$\mathcal{L}(\boldsymbol{a};\boldsymbol{U}) \doteq \left[\varrho(\boldsymbol{a}\cdot\nabla)\boldsymbol{u} - \mu\Delta\boldsymbol{u} - \frac{\mu}{3}\nabla(\nabla\cdot\boldsymbol{u}) + \nabla p,\ \frac{1}{\varrho c^2}(\boldsymbol{a}\cdot\nabla)p + \nabla\cdot\boldsymbol{u}\right]^\intercal,$$

for some advection velocity $\boldsymbol{a}$ and,

$$\mathcal{D}_t(\boldsymbol{U}) \doteq \left[\varrho\partial_t\boldsymbol{u},\ \frac{1}{\varrho c^2}\partial_t p\right]^\intercal,$$

we may state the strong form as,

$$\mathcal{D}_t(\boldsymbol{U}) + \mathcal{L}(\boldsymbol{u},\boldsymbol{U}) = \boldsymbol{F}.$$

The governing equations need to be complemented with a suitable set of both initial and boundary conditions to ensure the well-posedness of the problem, being the latter discussed in the next section. The initial conditions are set for velocity and pressure, and shall be written in the form $\boldsymbol{u} = \boldsymbol{u}^0$ and $p = p^0$ at time $t = 0$, being $\boldsymbol{u}^0$ and p^0 functions defined over the whole domain Ω. Note that (7)–(8) can be seen as a direct extension of the incompressible Navier–Stokes case with the addition of a temporal and convective term for the pressure.

The reader might have noticed that although several simplifications were introduced, the governing equations still depend on both density and sound velocity fields. In order to resolve these additional nonlinearities, (2) and (5) are used to complete the formulation and computed explicitly in time, so that one would need to solve only for velocity and pressure fields, as previously stated.

2.3. Variational form

Let us first introduce some notation. The space of square integrable functions in a domain ω will be denoted by $L^2(\omega)$. We shall also use $\langle f, g\rangle = \int_\omega fg$, where f and g are two generic functions defined on a region ω such that the integral of their product is well defined. Subscript ω will be omitted when $\omega = \Omega$. In addition to this, for a given Banach space X we write as $L^m(0, T; X)$ the Bochner

spaces of functions such that their X-norm is an $L^m(0, T)$ function in time, i.e., its m-th power is integrable if $1 \leq m < \infty$ or bounded if $m = \infty$. Finally, $\boldsymbol{n}$ will denote the geometric unit outward normal vector on the boundary $\Gamma = \partial\Omega$.

Let now V^d and Q be, respectively, the proper functional spaces where velocity and pressure solutions are well defined for each fixed time $t \in (0, T)$, with appropriate regularity not analyzed here. The weak form of the problem is derived by testing (7)-(8) against arbitrary test functions, namely $\boldsymbol{v} \in V^d$ and $q \in Q$. The variational problem prior to the application of boundary conditions written in a condensed manner reads: find $\boldsymbol{U} \in L^2(0, T; V^d \times Q)$ such that the initial conditions are satisfied and,

$$\langle \mathcal{D}_t(\boldsymbol{U}), \boldsymbol{V} \rangle + B(\boldsymbol{u}; \boldsymbol{U}, \boldsymbol{V}) = \langle \boldsymbol{v}, \boldsymbol{f} \rangle + \langle \boldsymbol{v}, \boldsymbol{n} \cdot \boldsymbol{\sigma}(\boldsymbol{u}, p) \rangle_\Gamma, \tag{9}$$

for all $\boldsymbol{V} \doteq [\boldsymbol{v}, q]^\intercal \in V^d \times Q$ and where,

$$\begin{aligned} B(\boldsymbol{u}; \boldsymbol{U}, \boldsymbol{V}) \doteq & \langle \varrho \boldsymbol{v}, (\boldsymbol{u} \cdot \nabla)\boldsymbol{u} \rangle + \mu \langle \nabla \boldsymbol{v}, \nabla \boldsymbol{u} \rangle \\ & + \frac{\mu}{3} \langle \nabla \cdot \boldsymbol{v}, \nabla \cdot \boldsymbol{u} \rangle - \langle \nabla \cdot \boldsymbol{v}, p \rangle \\ & + \left\langle q, \frac{1}{\varrho c^2} (\boldsymbol{u} \cdot \nabla) p \right\rangle + \langle q, \nabla \cdot \boldsymbol{u} \rangle. \end{aligned}$$

As usual, integration by parts was used and the stress tensor was identified as $\boldsymbol{\sigma}(\boldsymbol{u}, p) = -p\mathbf{I} + \mu \nabla \boldsymbol{u} + \frac{1}{3}\mu (\nabla \cdot \boldsymbol{u})\mathbf{I}$. Special care needs to be taken on the imposition of boundary conditions of the isentropic problem. This is to be treated next, so that the right hand side boundary term of (9) is modified in order to allow a compatible treatment of waves and flow velocity conditions.

3. Imposition of boundary conditions

Since the formulation we present aims at accounting for both flow and acoustic scales at once, there must be a compatibility requirement between the treatment of acoustic waves and the flow boundary conditions. In particular, a special type of condition must be imposed for the pressure field, whose main purpose is to allow the sound waves to leave the external boundaries of the computational domain smoothly. In this section we review the method proposed in [8] for the prescription of boundary conditions for the isentropic problem. The reader should note that the splitting of unknowns done in this section is a particularity of the technique to incorporate the boundary conditions and has nothing to do with the derivation of the fractional step method to be discussed later on.

3.1. Unknown and boundary splitting

The starting idea of the method is the splitting of the two unknown fields of the problem, i.e., velocity and pressure, into mean and oscillatory components. For a given time instant $t \in [0, T]$ and a point in the spatial domain $\boldsymbol{x} \in \Omega$, we have,

$$\boldsymbol{u}(\boldsymbol{x}, t) = \bar{\boldsymbol{u}}(\boldsymbol{x}, t) + \boldsymbol{u}'(\boldsymbol{x}, t), \qquad p(\boldsymbol{x}, t) = \bar{p}(\boldsymbol{x}, t) + p'(\boldsymbol{x}, t), \tag{10}$$

where the mean variables are mathematically described as,

$$\bar{\boldsymbol{u}}(\boldsymbol{x}, t) \doteq \frac{1}{T_w} \int_{t-T_w}^{t} \boldsymbol{u}(\boldsymbol{x}, \alpha)\, d\alpha, \qquad \bar{p}(\boldsymbol{x}, t) \doteq \frac{1}{T_w} \int_{t-T_w}^{t} p(\boldsymbol{x}, \alpha)\, d\alpha, \tag{11}$$

being T_w an appropriate time window. In the following, we will identify the oscillatory components with the acoustic fluctuations and the mean components with the flow variables. The main idea is that in (11), T_w implicitly defines a filtering frequency for the acoustic waves, which must be chosen small enough to allow a damping of the acoustic waves while still reproducing the flow behavior with certainty.

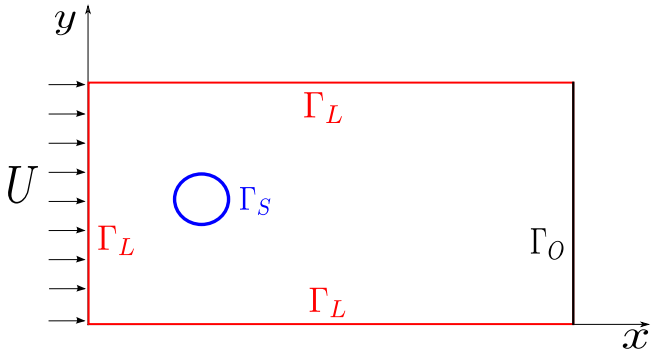

Fig. 1. Example of boundary splitting at the continuous level to allow a compatible prescription of boundary conditions. This setting corresponds to the examples presented in Sections 7.2 and 7.3.

Let us now introduce a boundary splitting at the continuous level, in order to manage the flow and acoustic boundary conditions in a suitable manner. The boundary $\Gamma = \partial\Omega$ is divided into three different disjoint subsets, namely, Γ_S, Γ_L and Γ_O (see Fig. 1). These subsets are such that $\Gamma_S \cap \Gamma_L = \emptyset$, $\Gamma_L \cap \Gamma_O = \emptyset$, $\Gamma_O \cap \Gamma_S = \emptyset$ and $\Gamma_S \cup \Gamma_L \cup \Gamma_O = \Gamma$. The boundary Γ_S refers to the solid boundary and Γ_L is identified with the lateral boundaries, i.e. any frontier with at least one component of the velocity prescribed to a known value. Finally, Γ_O stands for the outlet. On Γ_L and Γ_O, which are in the far field, it is assumed that the acoustic scales are dominant.

3.2. Unified prescription of boundary conditions

The two main ingredients of the methodology are: the weak prescription of essential boundary conditions and the application of Sommerfeld-like non-reflecting boundary conditions, NRBC. Next, we summarize the different conditions to be applied on each boundary.

On the solid boundary, i.e. Γ_S, the velocity is known and we apply:

$$\boldsymbol{u} = \bar{\boldsymbol{u}} + \boldsymbol{u}' = \boldsymbol{u}_s \quad \text{on} \quad \Gamma_S,$$

being $\boldsymbol{u}_s$ the prescribed velocity. This is a classical strong-Dirichlet type boundary.

On the frontiers belonging to the truncation boundary Γ_L, distinct conditions are enforced:

- The mean value of the velocity is prescribed to the flow inlet velocity,

  $$\bar{\boldsymbol{u}} = \boldsymbol{u}_L \quad \text{on} \quad \Gamma_L.$$

- A Sommerfeld-like non-reflecting boundary condition is prescribed for the acoustic component of the velocity field. In the normal direction to the boundary we define,

  $$\boldsymbol{n} \cdot \boldsymbol{u}' = -\frac{1}{\varrho c} \boldsymbol{n} \cdot [\boldsymbol{n} \cdot \boldsymbol{\sigma}(\boldsymbol{u}', p')] \quad \text{on} \quad \Gamma_L,$$

  and for the tangential direction we directly write,

  $$\boldsymbol{m} \cdot [\boldsymbol{n} \cdot \boldsymbol{\sigma}(\boldsymbol{u}', p')] = 0 \quad \text{on} \quad \Gamma_L,$$

  for any vector $\boldsymbol{m}$ in the tangent direction to Γ_L.

The prescription of $\bar{\boldsymbol{u}} = \boldsymbol{u}_L$ will be done weakly through the popular Nitsche's method [30] which provides a better conditioned problem. Finally, on the outflow boundary Γ_O, the following conditions are considered:

- The mean value tractions are prescribed to a value $\boldsymbol{t}_O$, i.e.,

  $$\boldsymbol{n} \cdot \boldsymbol{\sigma}(\bar{\boldsymbol{u}}, \bar{p}) = \boldsymbol{t}_O \quad \text{on} \quad \Gamma_O.$$

- The same approach as in Γ_L is used now for the fluctuating component. Then,

$$\boldsymbol{n}\cdot\boldsymbol{u}' = -\frac{1}{\varrho c}\boldsymbol{n}\cdot[\boldsymbol{n}\cdot\boldsymbol{\sigma}(\boldsymbol{u}', p')] \qquad \text{on} \quad \Gamma_O,$$
$$\boldsymbol{m}\cdot[\boldsymbol{n}\cdot\boldsymbol{\sigma}(\boldsymbol{u}', p')] = 0 \qquad \text{on} \quad \Gamma_O.$$

This is a boundary with natural conditions prescribed for $\bar{\boldsymbol{u}}$ and Sommerfeld conditions for $\boldsymbol{u}'$.

Taking now into account these definitions, the prescription of boundary conditions in the weak form of the problem can be done upon the modification of the right hand side term of (9). Thus,

$$\begin{aligned}\langle \boldsymbol{v}, \boldsymbol{n}\cdot\boldsymbol{\sigma}(\boldsymbol{u}, p)\rangle_\Gamma =& \langle \boldsymbol{v}, \boldsymbol{n}\cdot\boldsymbol{\sigma}(\boldsymbol{u}, p)\rangle_{\Gamma_L} + \langle \boldsymbol{v}, \boldsymbol{n}\cdot\boldsymbol{\sigma}(\boldsymbol{u}, p)\rangle_{\Gamma_O}\\ =& \langle \boldsymbol{v}, \boldsymbol{n}\cdot\boldsymbol{\sigma}(\bar{\boldsymbol{u}}, \bar{p})\rangle_{\Gamma_L} + \left\langle \boldsymbol{v}, \boldsymbol{n}\cdot\boldsymbol{\sigma}(\boldsymbol{u}', p')\right\rangle_{\Gamma_L}\\ &+ \langle \boldsymbol{v}, \boldsymbol{n}\cdot\boldsymbol{\sigma}(\bar{\boldsymbol{u}}, \bar{p})\rangle_{\Gamma_O} + \left\langle \boldsymbol{v}, \boldsymbol{n}\cdot\boldsymbol{\sigma}(\boldsymbol{u}', p')\right\rangle_{\Gamma_O},\end{aligned}$$

which after the introduction of the symmetrization and the penalty terms for the imposition of $\bar{\boldsymbol{u}} = \boldsymbol{u}_L$ via Nitsche's method reads,

$$\begin{aligned}\langle \boldsymbol{v}, \boldsymbol{n}\cdot\boldsymbol{\sigma}(\boldsymbol{u}, p)\rangle_\Gamma =& \langle \boldsymbol{v}, \boldsymbol{n}\cdot\boldsymbol{\sigma}(\bar{\boldsymbol{u}}, \bar{p})\rangle_{\Gamma_L} - \left\langle \boldsymbol{v}\cdot\boldsymbol{n}, \varrho c\boldsymbol{u}'\cdot\boldsymbol{n}\right\rangle_{\Gamma_L}\\ &+ \langle \bar{\boldsymbol{u}} - \boldsymbol{u}_L, \boldsymbol{n}\cdot\boldsymbol{\sigma}(\boldsymbol{v}, q)\rangle_{\Gamma_L},\\ &- \beta\langle \boldsymbol{v}, \bar{\boldsymbol{u}} - \boldsymbol{u}_L\rangle_{\Gamma_L} - \left\langle \boldsymbol{v}\cdot\boldsymbol{n}, \varrho c\boldsymbol{u}'\cdot\boldsymbol{n}\right\rangle_{\Gamma_O} + \langle \boldsymbol{v}, \boldsymbol{t}_O\rangle_{\Gamma_O},\end{aligned} \tag{12}$$

being β the numerical penalty parameter and with no contribution over Γ_S, since the condition is prescribed strongly on that boundary. It just remains to provide a definition of the outflow traction $\boldsymbol{t}_O$. Assuming that Γ_O is placed sufficiently far away from the solid boundary, i.e., in the far field-region, it is reasonable to set $\bar{p}\approx 0$ and $\nabla\bar{\boldsymbol{u}}\approx\boldsymbol{0}$ and hence the natural condition to be imposed is $\boldsymbol{t}_O = \boldsymbol{0}$. The reader should also note that there are several terms in (12) which are known and therefore can be taken to the right hand side of the problem. Let us group those boundary terms introducing the following forms,

$$\begin{aligned}&B_\Gamma(\boldsymbol{U}, \boldsymbol{V})\\ &\doteq \left\langle \boldsymbol{v}\cdot\boldsymbol{n}, \varrho c\boldsymbol{u}'\cdot\boldsymbol{n}\right\rangle_{\Gamma_L\cup\Gamma_O} - \langle \boldsymbol{v}, \boldsymbol{n}\cdot\boldsymbol{\sigma}(\bar{\boldsymbol{u}}, \bar{p})\rangle_{\Gamma_L} - \langle \bar{\boldsymbol{u}}, \boldsymbol{n}\cdot\boldsymbol{\sigma}(\boldsymbol{v}, q)\rangle_{\Gamma_L}\\ &\quad + \beta\langle \boldsymbol{v}, \bar{\boldsymbol{u}}\rangle_{\Gamma_L},\end{aligned} \tag{13}$$

$$L_\Gamma(\boldsymbol{V}) \doteq \beta\langle \boldsymbol{v}, \boldsymbol{u}_L\rangle_{\Gamma_L} - \langle \boldsymbol{u}_L, \boldsymbol{n}\cdot\boldsymbol{\sigma}(\boldsymbol{v}, q)\rangle_{\Gamma_L}, \tag{14}$$

which will go to the left and right hand side of the problem, respectively.

Finally, the variational formulation with the boundary conditions would now read as follows: find $\boldsymbol{U}\in L^2(0,\ T;\ V^d\times Q)$ such that,

$$\langle \mathcal{D}_t(\boldsymbol{U}), \boldsymbol{V}\rangle + B(\boldsymbol{u}; \boldsymbol{U}, \boldsymbol{V}) + B_\Gamma(\boldsymbol{U}, \boldsymbol{V}) = L(\boldsymbol{V}),$$

for all $\boldsymbol{V}\in V^d\times Q$, satisfying the initial conditions and where now $L(\boldsymbol{V}) \doteq L_\Gamma(\boldsymbol{V}) + \langle \boldsymbol{v}, \boldsymbol{f}\rangle$.

4. Numerical approximation

In this section we derive the finite element approximation of the isentropic compressible Navier–Stokes equations, which is the base of the final segregation scheme.

4.1. Galerkin finite element approximation

Let $\mathcal{T}_h(\Omega)$ be a regular-shaped and conforming partition of Ω, such that $\overline{\Omega} = \cup_{K\in\mathcal{T}_h} K$. This triangulation is described by the characteristic mesh size, defined as $h \doteq \max\{h_k \mid K\in\mathcal{T}_h(\Omega)\}$ with $h_K = \text{diam}(K)$. Let now be $V_h^d \subset V^d$ and $Q_h \subset Q$ the velocity and pressure finite element spaces associated with the triangulation. The Galerkin semi-discrete problem consits in finding $\boldsymbol{U}_h \doteq [\boldsymbol{u}_h, p_h]^\intercal \in L^2(0, T; V_h^d\times Q_h)$ such that,

$$\langle \mathcal{D}_t(\boldsymbol{U}_h), \boldsymbol{V}_h\rangle + B(\boldsymbol{u}_h; \boldsymbol{U}_h, \boldsymbol{V}_h) + B_\Gamma(\boldsymbol{U}_h, \boldsymbol{V}_h) = L(\boldsymbol{V}_h), \tag{15}$$

for all $\boldsymbol{V}_h \doteq [\boldsymbol{v}_h, q_h]^\intercal \in V_h^d\times Q_h$, satisfying the appropriate initial conditions.

As we shall see at the end of this section and in contrast to the classical incompressible case, the algebraic system arising from the discrete isentropic problem is no longer of the saddle point type, yet some prerequisites might be needed so as to ensure that the matrix of the whole system has a full rank. Likewise, instabilities may also arise due to the presence of the convective terms. For the sake of simplicity, and without loss of generality, we will assume for the moment that the Galerkin formulation is stable. Later, in Section 6, we will deeply describe the stabilized finite element formulation we favor, which allows one to solve highly convective cases.

4.2. Monolithic time discretization

We restrict ourselves to the classical backward-difference (BDF) approximation for clearness in the discussion, yet in principle any time discretization method might be used to advance the solution in time. Let us now consider a partition of the time interval [0, T] into N time steps of size δt, assumed to be constant, for simplicity. Given a generic time dependent function $g(t)$ at a time step $t^{n+1} = t^n + \delta t$, for $n = 0, 1, 2, \ldots$, the approximation of the time derivative of $g(t)$ of order $k = 1, 2, \ldots$ is written as $\delta_k g^{n+1}/\delta t$, where the numerator is given by the following BDF operator,

$$\delta_k g^{n+1} = \frac{1}{\psi_k}\left(g^{n+1} - \sum_{i=0}^{k-1}\xi_k^i g^{n-i}\right),$$

being ψ_k and ξ_k^i numerical parameters depending on the order of the temporal approximation. In particular, for the first and second order schemes, i.e. $k = 1, 2$, it is found that:

$$\delta_1 g^{n+1} = \delta g^{n+1} = g^{n+1} - g^n,$$
$$\delta_2 g^{n+1} = \frac{3}{2}\left(g^{n+1} - \frac{4}{3}g^n + \frac{1}{3}g^{n-1}\right).$$

In the design of fractional step schemes, it is useful to define the extrapolation operators of order k, formally written as $\hat{g}_k^{n+1} = g^{n+1} + \mathcal{O}(\delta t^k)$, which for $k = 1, 2$ are given by,

$$\hat{g}_1^{n+1} = g^n, \tag{16}$$

$$\hat{g}_2^{n+1} = 2g^n - g^{n-1}. \tag{17}$$

Using the aforementioned BDF schemes, the time discretization of the semi-discrete Eq. (15) is stated as: for $n = 0, 1, 2, \ldots$, find $\boldsymbol{U}^{n+1} \in V_h^d\times Q_h$ such that,

$$\left\langle \mathcal{D}_{t,k}(\boldsymbol{U}_h^{n+1}), \boldsymbol{V}_h\right\rangle + B(\boldsymbol{u}_h^{n+1}; \boldsymbol{U}_h^{n+1}, \boldsymbol{V}_h) + B_\Gamma(\boldsymbol{U}_h^{n+1}, \boldsymbol{V}_h) = L(\boldsymbol{V}_h), \tag{18}$$

for all test functions. For the sake of clarity, we include also the expanded discrete problem, i.e., for $n = 0, 1, 2, \ldots$, find $\boldsymbol{u}_h^{n+1},\ p_h^{n+1} \in V_h^d\times Q_h$ such that,

$$\left\langle \boldsymbol{v}_h, \varrho^{n+1}\frac{\delta_k \boldsymbol{u}_h^{n+1}}{\delta t}\right\rangle + \left\langle \varrho^{n+1}\boldsymbol{v}_h, (\boldsymbol{u}_h^{n+1}\cdot\nabla)\boldsymbol{u}_h^{n+1}\right\rangle + \mu\left\langle \nabla \boldsymbol{v}_h, \nabla \boldsymbol{u}_h^{n+1}\right\rangle$$
$$+ \frac{\mu}{3}\left\langle \nabla\cdot\boldsymbol{v}_h, \nabla\cdot\boldsymbol{u}_h^{n+1}\right\rangle - \left\langle \nabla\cdot\boldsymbol{v}_h, p_h^{n+1}\right\rangle$$
$$+ \left\langle \boldsymbol{v}_h\cdot\boldsymbol{n}, \varrho^{n+1}c^{n+1}\boldsymbol{u}_h'^{n+1}\cdot\boldsymbol{n}\right\rangle_{\Gamma_L\cup\Gamma_O} + \left\langle \boldsymbol{v}_h\cdot\boldsymbol{n}, \bar{p}_h^{n+1}\right\rangle_{\Gamma_L}$$
$$- \mu\left\langle \boldsymbol{v}_h, \boldsymbol{n}\cdot\nabla\bar{\boldsymbol{u}}_h^{n+1}\right\rangle_{\Gamma_L} - \frac{\mu}{3}\left\langle \boldsymbol{v}_h\cdot\boldsymbol{n}, \nabla\cdot\bar{\boldsymbol{u}}_h^{n+1}\right\rangle_{\Gamma_L} + \beta\left\langle \boldsymbol{v}_h, \bar{\boldsymbol{u}}_h^{n+1}\right\rangle_{\Gamma_L}$$
$$- \mu\left\langle \boldsymbol{n}\cdot\nabla\boldsymbol{v}_h, \bar{\boldsymbol{u}}_h^{n+1}\right\rangle_{\Gamma_L} - \frac{\mu}{3}\left\langle \nabla\cdot\boldsymbol{v}_h, \bar{\boldsymbol{u}}_h^{n+1}\cdot\boldsymbol{n}\right\rangle_{\Gamma_L} = \beta\langle \boldsymbol{v}_h, \boldsymbol{u}_L\rangle_{\Gamma_L}$$
$$- \mu\langle \boldsymbol{n}\cdot\nabla\boldsymbol{v}_h, \boldsymbol{u}_L\rangle_{\Gamma_L} - \frac{\mu}{3}\langle \nabla\cdot\boldsymbol{v}_h, \boldsymbol{u}_L\cdot\boldsymbol{n}\rangle_{\Gamma_L} + \langle \boldsymbol{v}_h, \boldsymbol{f}\rangle, \tag{19}$$

$$\left\langle q_h, \frac{1}{\varrho^{n+1}\left(c^2\right)^{n+1}}\frac{\delta_k p_h^{n+1}}{\delta t}\right\rangle + \left\langle q_h, \frac{1}{\varrho^{n+1}\left(c^2\right)^{n+1}}\left(\boldsymbol{u}_h^{n+1}\cdot\nabla\right)p_h^{n+1}\right\rangle$$
$$+ \left\langle q_h, \nabla\cdot\boldsymbol{u}_h^{n+1}\right\rangle + \left\langle q_h, \bar{\boldsymbol{u}}_h^{n+1}\cdot\boldsymbol{n}\right\rangle_{\Gamma_L} = \langle q_h, \boldsymbol{u}_L\cdot\boldsymbol{n}\rangle_{\Gamma_L}, \tag{20}$$

for all $\boldsymbol{v}_h,\ q_h \in V_h^d \times Q_h$.

Regarding the boundary condition terms, it remains to provide a discrete expression to compute the mean components of the unknowns. At the discrete level, the time window introduced in (11) is computed as $T_w = N_w\delta t$ being N_w a certain amount of time steps. It is proposed to use the trapezoidal rule for integration in order to compute the mean variables. The expression we use for the average values is,

$$\bar{\boldsymbol{u}}_h^{n+1} = \frac{\delta t}{T_w}\left(\frac{1}{2}\boldsymbol{u}_h^{n+1} + \sum_{j=n-N_w+2}^{n}\boldsymbol{u}_h^{j} + \frac{1}{2}\boldsymbol{u}_h^{n-N_w+1}\right),$$

and equivalently for the pressure. This expression maintains the integration implicit and second order accurate, but several time steps need to be run prior to its application so as to obtain representative data for a reliable mean computation.

4.3. Monolithic algebraic system

The fully discretized equations in (19)-(20) provide an algebraic system for the nodal values of the finite element unknowns, i.e. $[\boldsymbol{u}_h^{n+1}, p_h^{n+1}]$. In order to get this final finite element matrix problem, we simply need to substitute the finite element approximation of the unknowns and the analogous for the test functions $\boldsymbol{v}_h$, q_h. If P^{n+1} denotes the unknown nodal pressure values and U^{n+1} the unknown nodal velocity values at each time step, the algebraic structure of the variational formulation (18) results in,

$$\mathsf{M}_{\boldsymbol{u}}\frac{\delta_k}{\delta t}\mathsf{U}^{n+1} + \mathsf{K}_{\boldsymbol{u}}(\mathsf{U}^{n+1})\mathsf{U}^{n+1} + \mathsf{M}_\Gamma\mathsf{U}^{n+1} + \mathsf{K}_\Gamma\mathsf{U}^{n+1}$$
$$+ \mathsf{G}\mathsf{P}^{n+1} + \mathsf{G}_\Gamma\mathsf{P}^{n+1} = \mathsf{F}^{n+1} + \mathsf{F}_{\Gamma,\boldsymbol{u}}^{n+1}, \tag{21}$$

$$\mathsf{M}_p\frac{\delta_k}{\delta t}\mathsf{P}^{n+1} + \mathsf{K}_p(\mathsf{U}^{n+1})\mathsf{P}^{n+1} + \mathsf{D}\mathsf{U}^{n+1} + \mathsf{D}_\Gamma\mathsf{U}^{n+1} = \mathsf{F}_{\Gamma,p}^{n+1}, \tag{22}$$

where subscripts $(\cdot)_{\boldsymbol{u}}$ and $(\cdot)_p$ refer to matrices of the momentum and continuity equation. The dependence of matrices $\mathsf{K}_{\boldsymbol{u}}$ and K_p on the vector of velocity unknowns has been explicitly displayed in order to remark the nonlinear character of the problem. In addition, $(\cdot)_\Gamma$ stands for terms arising from the special treatment of boundary conditions, with M_Γ containing the penalty term and $\mathsf{K}_\Gamma, \mathsf{G}_\Gamma$ and D_Γ the remaining Nitsche and Sommerfeld contributions. It is straightforward to identify the rest of arrays in (21)-(22) and the expressions in (19)-(20).

5. Design of the fractional step method

The approach chosen in this work is to introduce a segregation technique at the pure algebraic level, as done for instance in [31] for the viscoelastic flow problem, in contrast to the space continuous level. Although specific boundary conditions were discussed for the isentropic problem in order to avoid the backscattering of sound waves, the adopted algebraic viewpoint precludes a further analysis on the correct pressure boundary conditions for the different stages of the fractional step algorithm.

5.1. Pressure-correction algorithm

The method we propose in this section is directly linked to a pressure-correction scheme applied to the incompressible flow problem, in which a velocity guess is first computed and then corrected once the pressure is calculated. Another possibility would be to calculate first a pressure guess, what would provide a velocity-correction-like algorithm. We will not discuss them here, yet the ideas presented next could be also used to design velocity-correction schemes (see [11] and references therein).

In order to derive the method, let us start by writing system (21)-(22) in the following *equivalent* manner,

$$\mathsf{M}_{\boldsymbol{u}}\frac{\delta_k}{\delta_t}\widetilde{\mathsf{U}}^{n+1} + \mathsf{K}_{\boldsymbol{u}}(\widetilde{\mathsf{U}}^{n+1})\widetilde{\mathsf{U}}^{n+1} + \mathsf{M}_\Gamma\widetilde{\mathsf{U}}^{n+1} + \mathsf{K}_\Gamma\widetilde{\mathsf{U}}^{n+1}$$
$$+ (\mathsf{G}+\mathsf{G}_\Gamma)\widehat{\mathsf{P}}_{k'}^{n+1} = \mathsf{F}^{n+1} + \mathsf{F}_{\Gamma,\boldsymbol{u}}^{n+1}, \tag{23}$$

$$\frac{1}{\psi_k\delta t}\mathsf{M}_{\boldsymbol{u}}(\mathsf{U}^{n+1} - \widetilde{\mathsf{U}}^{n+1}) + \mathsf{N}_{\boldsymbol{u}}^{n+1} + \mathsf{N}_\beta^{n+1} + \mathsf{N}_\Gamma^{n+1}$$
$$+ (\mathsf{G}+\mathsf{G}_\Gamma)(\mathsf{P}^{n+1} - \widehat{\mathsf{P}}_{k'}^{n+1}) = 0, \tag{24}$$

$$\mathsf{M}_p\frac{\delta_k}{\delta_t}\mathsf{P}^{n+1} + \mathsf{K}_p(\mathsf{U}^{n+1})\mathsf{P}^{n+1} - \psi_k\delta t(\mathsf{D}+\mathsf{D}_\Gamma)\mathsf{M}_{\boldsymbol{u}}^{-1}\mathsf{N}_{\boldsymbol{u}}^{n+1}$$
$$- \psi_k\delta t(\mathsf{D}+\mathsf{D}_\Gamma)\mathsf{M}_{\boldsymbol{u}}^{-1}\mathsf{N}_\beta^{n+1} - \psi_k\delta t(\mathsf{D}+\mathsf{D}_\Gamma)\mathsf{M}_{\boldsymbol{u}}^{-1}\mathsf{N}_\Gamma^{n+1}$$
$$- \psi_k\delta t(\mathsf{D}+\mathsf{D}_\Gamma)\mathsf{M}_{\boldsymbol{u}}^{-1}(\mathsf{G}+\mathsf{G}_\Gamma)(\mathsf{P}^{n+1} - \widehat{\mathsf{P}}_{k'}^{n+1})$$
$$+ (\mathsf{D}+\mathsf{D}_\Gamma)\widetilde{\mathsf{U}}^{n+1} = \mathsf{F}_{\Gamma,p}^{n+1}, \tag{25}$$

where,

$$\mathsf{N}_{\boldsymbol{u}}^{n+1} = \mathsf{K}_{\boldsymbol{u}}(\mathsf{U}^{n+1})\mathsf{U}^{n+1} - \mathsf{K}_{\boldsymbol{u}}(\widetilde{\mathsf{U}}^{n+1})\widetilde{\mathsf{U}}^{n+1},$$
$$\mathsf{N}_\beta^{n+1} = \mathsf{M}_\Gamma\mathsf{U}^{n+1} - \mathsf{M}_\Gamma\widetilde{\mathsf{U}}^{n+1},$$
$$\mathsf{N}_\Gamma^{n+1} = \mathsf{K}_\Gamma\mathsf{U}^{n+1} - \mathsf{K}_\Gamma\widetilde{\mathsf{U}}^{n+1},$$

and $\widetilde{\mathsf{U}}^{n+1}$ is an auxiliary variable to which we shall refer as intermediate velocity. Likewise, $\widehat{\mathsf{P}}_{k'}^{n+1}$ is an extrapolation of the pressure of order k' at time step t^{n+1}. See (16)-(17) for details. The reader should note that adding up (23) and (24) we recover (21), and that (25) is derived upon substitution into (22) of the relation between U^{n+1} and $\widetilde{\mathsf{U}}^{n+1}$ obtained from (24). Generally speaking, the fractional step approach to solve the isentropic compressible Navier–Stokes problem involves three steps: first compute the intermediate velocity from (23), then obtain the pressure from (25), and finally correct the velocity result using (24).

This scheme will make possible to segregate the calculation of the unknowns of the problem and provides a pressure-correction-like algorithm. However, some extra information is needed since Eqs. (24) and (25) still couple U^{n+1} and P^{n+1}. At this point, it is very convenient to make the following observations:

Remark 5.1. One should notice that the resulting matrix from $\mathsf{D}\mathsf{M}_{\boldsymbol{u}}^{-1}\mathsf{G}$ in (25) can be viewed as an approximation to the discrete version of the Laplacian operator $\Delta(\cdot)$, [32]. In order to avoid dealing with this matrix, which has a wide stencil and might be computationally feasible only if $\mathsf{M}_{\boldsymbol{u}}$ is approximated by a diagonal matrix, we can work with $\mathsf{D}\mathsf{M}_{\boldsymbol{u}}^{-1}\mathsf{G} \approx \mathsf{L}$ where L is a Laplacian matrix obtained using the gradient of the standard shape functions.

Algorithm 1 First and second order fractional step scheme for the isentropic problem, $k = 1, 2$.

1. Nonlinear problem to compute the intermediate velocity $\widetilde{\mathrm{U}}^{n+1}$using the pressure extrapolations:

$$\mathrm{M}_{\boldsymbol{u}}\frac{\delta_k}{\delta t}\widetilde{\mathrm{U}}^{n+1} + \mathrm{K}_{\boldsymbol{u}}(\widetilde{\mathrm{U}}^{n+1})\widetilde{\mathrm{U}}^{n+1} + \mathrm{M}_{\Gamma}\widetilde{\mathrm{U}}^{n+1} + \mathrm{K}_{\Gamma}\widetilde{\mathrm{U}}^{n+1} = \mathrm{F}^{n+1} + \mathrm{F}^{n+1}_{\Gamma,\boldsymbol{u}} - \mathrm{G}\widehat{\mathrm{P}}^{n+1}_{k-1} - \mathrm{G}_{\Gamma}\widehat{\mathrm{P}}^{n+1}_{k}$$

2. Compute the pressure P^{n+1} using the intermediate velocityfrom the previous step:

$$\mathrm{M}_{p}\frac{\delta_k}{\delta t}\mathrm{P}^{n+1} + \mathrm{K}_{p}(\widetilde{\mathrm{U}}^{n+1})\mathrm{P}^{n+1} - \psi_k\delta t\mathrm{L}\mathrm{P}^{n+1} = \mathrm{F}^{n+1}_{\Gamma,p} - \mathrm{D}\widetilde{\mathrm{U}}^{n+1} - \mathrm{D}_{\Gamma}\widehat{\mathrm{U}}^{n+1}_{k} - \psi_k\delta t\mathrm{L}\widehat{\mathrm{P}}^{n+1}_{k-1}$$

3. Velocity correction to obtain the end-of-step velocity U^{n+1}:

$$\frac{1}{\psi_k\delta t}\mathrm{M}_{\boldsymbol{u}}\mathrm{U}^{n+1} + \mathrm{M}_{\Gamma}\mathrm{U}^{n+1} = \frac{1}{\psi_k\delta t}\mathrm{M}_{\boldsymbol{u}}\widetilde{\mathrm{U}}^{n+1} + \mathrm{M}_{\Gamma}\widetilde{\mathrm{U}}^{n+1} - \mathrm{G}(\mathrm{P}^{n+1} - \widehat{\mathrm{P}}^{n+1}_{k-1})$$

Remark 5.2. If we wanted to compute the pressure from Eq. (25), we would still have to face the difficulty of computing terms such as $\mathrm{D}_{\Gamma}\mathrm{M}_{\boldsymbol{u}}^{-1}\mathrm{G}$, $\mathrm{D}\mathrm{M}_{\boldsymbol{u}}^{-1}\mathrm{G}_{\Gamma}$ and $\mathrm{D}_{\Gamma}\mathrm{M}_{\boldsymbol{u}}^{-1}\mathrm{G}_{\Gamma}$. Such computations can be really time consuming and burdensome. Note that an approximation similar to the one just commented above is not possible due to the character of the boundary matrices D_{Γ} and G_{Γ}.

5.2. Explicit treatment of boundary terms and final segregated scheme

Having the previous information in mind, the novel idea we propose in this work is to modify (23) and (25) in such a way that both boundary terms $\mathrm{G}_{\Gamma}\mathrm{P}^{n+1}$ and $\mathrm{D}_{\Gamma}\mathrm{U}^{n+1}$ are treated explicitly, by means of an extrapolation of the same order of the time integration scheme, k. This implies that system (23)-(25) would now read,

$$\begin{aligned}&\mathrm{M}_{\boldsymbol{u}}\frac{\delta_k}{\delta_t}\widetilde{\mathrm{U}}^{n+1} + \mathrm{K}_{\boldsymbol{u}}(\widetilde{\mathrm{U}}^{n+1})\widetilde{\mathrm{U}}^{n+1} + \mathrm{M}_{\Gamma}\widetilde{\mathrm{U}}^{n+1} + \mathrm{K}_{\Gamma}\widetilde{\mathrm{U}}^{n+1} + \mathrm{G}\widehat{\mathrm{P}}^{n+1}_{k'}\\ &\quad + \mathrm{G}_{\Gamma}\widehat{\mathrm{P}}^{n+1}_{k} = \mathrm{F}^{n+1} + \mathrm{F}^{n+1}_{\Gamma,\boldsymbol{u}},\end{aligned} \tag{26}$$

$$\frac{1}{\psi_k\delta t}\mathrm{M}_{\boldsymbol{u}}(\mathrm{U}^{n+1} - \widetilde{\mathrm{U}}^{n+1}) + \mathrm{N}^{n+1}_{\boldsymbol{u}} + \mathrm{N}^{n+1}_{\beta} + \mathrm{N}^{n+1}_{\Gamma} + \mathrm{G}(\mathrm{P}^{n+1} - \widehat{\mathrm{P}}^{n+1}_{k'}) = 0, \tag{27}$$

$$\begin{aligned}&\mathrm{M}_{p}\frac{\delta_k}{\delta_t}\mathrm{P}^{n+1} + \mathrm{K}_{p}(\mathrm{U}^{n+1})\mathrm{P}^{n+1} - \psi_k\delta t(\mathrm{D}+\mathrm{D}_{\Gamma})\mathrm{M}_{\boldsymbol{u}}^{-1}\mathrm{N}^{n+1}_{\boldsymbol{u}}\\ &\quad - \psi_k\delta t(\mathrm{D}+\mathrm{D}_{\Gamma})\mathrm{M}_{\boldsymbol{u}}^{-1}\mathrm{N}^{n+1}_{\beta} - \psi_k\delta t(\mathrm{D}+\mathrm{D}_{\Gamma})\mathrm{M}_{\boldsymbol{u}}^{-1}\mathrm{N}^{n+1}_{\Gamma}\\ &\quad - \psi_k\delta t\mathrm{D}\mathrm{M}_{\boldsymbol{u}}^{-1}\mathrm{G}(\mathrm{P}^{n+1} - \widehat{\mathrm{P}}^{n+1}_{k'}) + \mathrm{D}\widetilde{\mathrm{U}}^{n+1} + \mathrm{D}_{\Gamma}\widehat{\mathrm{U}}^{n+1}_{k} = \mathrm{F}^{n+1}_{\Gamma,p}.\end{aligned} \tag{28}$$

Note that now the products $\mathrm{D}_{\Gamma}\mathrm{M}_{\boldsymbol{u}}^{-1}\mathrm{G}$, $\mathrm{D}\mathrm{M}_{\boldsymbol{u}}^{-1}\mathrm{G}_{\Gamma}$ and $\mathrm{D}_{\Gamma}\mathrm{M}_{\boldsymbol{u}}^{-1}\mathrm{G}_{\Gamma}$ do not appear in the formulation and that we treat some terms on the boundary explicitly via extrapolations in $\mathrm{G}_{\Gamma}\widehat{\mathrm{P}}^{n+1}_{k}$ and $\mathrm{D}_{\Gamma}\widehat{\mathrm{U}}^{n+1}_{k}$. Formally, the fractional step algorithm of order k can be stated by taking $k' = k - 1$ and it entails the following steps:

1. Compute an intermediate velocity $\widetilde{\mathrm{U}}^{n+1}$ from (26).
2. Compute an approximation to the pressure P^{n+1} from (28) neglecting $\mathrm{N}^{n+1}_{\boldsymbol{u}}$, $\mathrm{N}^{n+1}_{\beta}\mathrm{N}^{n+1}_{\Gamma}$ and substituting U^{n+1} by $\widetilde{\mathrm{U}}^{n+1}$ in the term $\mathrm{K}_{p}(\mathrm{U}^{n+1})\mathrm{P}^{n+1}$. It can be seen that formally this perturbation is of order $\mathcal{O}(\delta t^k)$. It is the key point that permits to uncouple the calculation of U^{n+1} and P^{n+1}.
3. Perform the correction and compute the end-of-step velocity U^{n+1} from (27) neglecting $\mathrm{N}^{n+1}_{\boldsymbol{u}}$, $\mathrm{N}^{n+1}_{\Gamma}$ but taking into account N^{n+1}_{β}. This can be seen as a sort of Yosida factorization for the imposition of boundary conditions.

It is well known that the extrapolation of second order of the term $\mathrm{G}\widehat{\mathrm{P}}^{n+1}_{k'}$, i.e., taking $k' = 2$, is unstable (see [11] and references inside). Hence the resulting scheme is known to be stable up to $k = 2$. In fact, this issue motivated the study of velocity correction algorithms, which allow to design fractional step schemes of third order in time straightforwardly. Still, we did not observe any erratic behaviour of the term $\mathrm{G}_{\Gamma}\widehat{\mathrm{P}}^{n+1}_{k}$ for the extrapolation of second order. The final algorithm in its matrix form is included in Algorithm 1.

Although the previous technique provides a practical way to segregate the computations while accounting for a weak imposition of boundary conditions, some errors are introduced which can compromise the accuracy of the solution. The first error is due to the fact that the momentum Eq. (26) is solved for the intermediate velocity $\widetilde{\mathrm{U}}^{n+1}$ instead of the end of step velocity U^{n+1}. On top of that, an extra Dirichlet boundary condition needs to be provided for the second step. The essential boundary condition we enforce (at the continuous level) is:

$$\begin{aligned}&\bar{p} = 0 && \text{in } \Gamma_O,\\ &p' = \varrho c(\boldsymbol{u}'\cdot\boldsymbol{n}) && \text{in } \Gamma_O,\end{aligned} \tag{29}$$

where we take into account the decomposition of the pressure in average (flow) and oscillatory (acoustic) components as suggested in Section 3. Eq. (29) aids to enforce the NRBC when solving the continuity equation.

The inclusion of the penalization correction N^{n+1}_{β} in the last step of the algorithm aids to properly impose the boundary conditions of the problem avoiding boundary instabilities. It seems reasonable to take it into account, bearing in mind that the splitting of the momentum equation in (26)-(28) needs to be done taking into account boundary conditions, similarly to the case in which boundary conditions are enforced strongly. It is also important to note that M_{Γ} displays a structure of mass matrix but for boundary contributions, what in turn would allow to solve directly the system for U^{n+1} if a lumping technique is used. Moreover, the correction of the convective term $\mathrm{N}^{n+1}_{\boldsymbol{u}}$ could also be taken into consideration in this last step, yielding a complete Yosida scheme. This would permit to derive a high order method in time (see [11], Section 4.3).

Finally, another possibility for the extrapolation of the velocity boundary term could be argued. Since $\widetilde{\mathrm{U}}^{n+1}$ is an approximation of $\mathcal{O}(\delta t^k)$ to U^{n+1}, and the intermediate velocity is already computed when the term $\mathrm{D}_{\Gamma}\mathrm{U}^{n+1}$ needs to be treated explicitly, one could even consider to compute $\mathrm{D}_{\Gamma}\widetilde{\mathrm{U}}^{n+1}$ instead of $\mathrm{D}_{\Gamma}\widehat{\mathrm{U}}^{n+1}_{k}$. Numerical experiments show that both options provide comparable results.

6. Isentropic-compressible stabilized finite element formulation

The last part of a robust formulation consists in developing an appropriate stabilization scheme which enables to solve highly convective problems, thus avoiding spurious solutions. Apart from

that, it is helpful to use formulations which permit arbitrary velocity-pressure interpolations, not neccessarily satisfying any inf-sup-like condition. The stabilized formulation we propose in this work is within the VMS framework and, in particular, it is based on the Orthogonal Subgrid Scale concept (see [33] for a detailed review with examples of application).

6.1. Variational mulsti-scale framework: the subscale concept

Let us start by considering a general transient nonlinear problem, which we will use to illustrate the VMS procedure. Let us analyze,

$$M(\boldsymbol{U})\partial_t \boldsymbol{U} + \mathcal{L}(\boldsymbol{U},\boldsymbol{U}) = \mathbf{F},$$

being $\boldsymbol{U}$ the unknown, $M(\boldsymbol{U})$ a matrix of coefficients associated to the temporal term (possibly nonlinear in the most general case), $\mathbf{F}$ is any possible right hand side field and $\mathcal{L}(\boldsymbol{U},\cdot)$ a spatial differential operator, linear in the second argument. The weak form of this evolution problem is formally stated as: find $\boldsymbol{U}$: $(0,\ T)\to W$, such that,

$$(M(\boldsymbol{U})\partial_t \boldsymbol{U}, \boldsymbol{V}) + \langle \mathcal{L}(\boldsymbol{U},\boldsymbol{U}), \boldsymbol{V}\rangle = \langle \mathbf{F}, \boldsymbol{V}\rangle, \tag{30}$$

for any test function $\boldsymbol{V}\in W$ with appropriate regularity. Any possible terms that might arise from the imposition of boundary conditions need to be taken into account and the reader should understand that are incorporated in the duality $\langle\cdot,\cdot\rangle$.

The starting idea of the VMS methods is to consider a splitting of the space W of the form $W = W_h \oplus \check{W}$, that is to say, a decomposition into a finite element part W_h and any complementary space to it $\check{W}$, usually termed subgrid space. Such decomposition induces a scale separation of unknowns and associated test functions, i.e., $\boldsymbol{U} = \boldsymbol{U}_h + \check{\boldsymbol{U}}$ and $\boldsymbol{V} = \boldsymbol{V}_h + \check{\boldsymbol{V}}$, such that $\boldsymbol{U}_h$, $\boldsymbol{V}_h \in W_h$ and $\check{\boldsymbol{U}}, \check{\boldsymbol{V}} \in \check{W}$. The aforementioned decomposition at the continuous level of spaces, unknowns and test functions implies that one could divide (30) into two subproblems. Therefore,

$$(M(\boldsymbol{U})\partial_t \boldsymbol{U}, \boldsymbol{V}_h) + \langle \mathcal{L}(\boldsymbol{U},\boldsymbol{U}), \boldsymbol{V}_h\rangle = \langle \mathbf{F}, \boldsymbol{V}_h\rangle \qquad \forall \boldsymbol{V}_h \in W_h, \tag{31}$$

$$\left(M(\boldsymbol{U})\partial_t \boldsymbol{U}, \check{\boldsymbol{V}}\right) + \left\langle \mathcal{L}(\boldsymbol{U},\boldsymbol{U}), \check{\boldsymbol{V}}\right\rangle = \left\langle \mathbf{F}, \check{\boldsymbol{V}}\right\rangle \qquad \forall \check{\boldsymbol{V}} \in \check{W}. \tag{32}$$

System (31)-(32) is exactly equivalent to the prior weak form (30). Eq. (31) is referred as the equation for the finite element unknowns whereas (32) is termed the equation for the subgrid scales.

6.2. Derivation of the subscale stabilized formulation

The objective of this technique is to define an expression to numerically compute the subscales by solving (32) so that once this is introduced into (31), we end up with only a problem for the finite element unknowns $\boldsymbol{U}_h$. However, several approximations have to be made since the subgrid space $\check{W}$ is in principle infinite dimensional. Although not enough to define a numerical scheme, subcales are usually modeled as bubble functions and thus inter-element terms are neglected.

Applying integration by parts to isolate the subscale variables, Eqs. (31)-(32) can be rewritten as follows,

$$(M(\boldsymbol{U})\partial_t \boldsymbol{U}, \boldsymbol{V}_h) + \langle \mathcal{L}(\boldsymbol{U},\boldsymbol{U}_h), \boldsymbol{V}_h\rangle + \left\langle \check{\boldsymbol{U}}, \mathcal{L}^*(\boldsymbol{U},\boldsymbol{V}_h)\right\rangle = \langle \mathbf{F}, \boldsymbol{V}_h\rangle \quad \forall \boldsymbol{V}_h \in W_h, \tag{33}$$

$$\left(M(\boldsymbol{U})\partial_t \boldsymbol{U}, \check{\boldsymbol{V}}\right) + \left\langle \mathcal{L}(\boldsymbol{U},\boldsymbol{U}_h), \check{\boldsymbol{V}}\right\rangle + \left\langle \mathcal{L}(\boldsymbol{U},\check{\boldsymbol{U}}), \check{\boldsymbol{V}}\right\rangle = \left\langle \mathbf{F}, \check{\boldsymbol{V}}\right\rangle \qquad \forall \check{\boldsymbol{V}} \in \check{W}, \tag{34}$$

where $\mathcal{L}^*(\boldsymbol{U},\cdot)$ refers to the formal adjoint of the spatial operator $\mathcal{L}(\boldsymbol{U},\cdot)$. Similarly as the finite element Eq. (31) can be understood as the projection of the original equations onto the finite element space, the equations for the subscales are obtained by projecting the original equations onto the corresponding space. Therefore, Eq. (34) could be rewritten as,

$$\check{P}\left[M(\boldsymbol{U})\partial_t \check{\boldsymbol{U}} + \mathcal{L}(\boldsymbol{U},\check{\boldsymbol{U}})\right] = \check{P}[\boldsymbol{R}(\boldsymbol{U};\boldsymbol{U}_h)],$$

where the symbol $\check{P}[\cdot]$ stands for the linear projection operator onto the space of subscales and $\boldsymbol{R}(\boldsymbol{U};\boldsymbol{U}_h) \doteq \mathbf{F} - \mathcal{L}(\boldsymbol{U},\boldsymbol{U}_h) - M(\boldsymbol{U})\partial_t \boldsymbol{U}_h$ is identified with the finite element residual.

The additional assumption is based on replacing the spatial operator $\mathcal{L}(\boldsymbol{U},\cdot)$ by an algebraic operator which could be computed somehow and inverted and so that the new terms have approximately the same L^2-norm as the replaced ones. This fact motivates the introduction of a matrix $\boldsymbol{\tau}$, usually referred as matrix of stabilization parameters and defined element-wise in such a way that the following approximation is made,

$$\mathcal{L}(\boldsymbol{U},\check{\boldsymbol{U}}) \approx \boldsymbol{\tau}^{-1}(\boldsymbol{U})\check{\boldsymbol{U}}. \tag{35}$$

With the abovementioned assumption, the subscales could be computed in each element $K \in \mathcal{T}_h(\Omega)$ by solving the following nonlinear ordinary differential equation,

$$M(\boldsymbol{U})\partial_t \check{\boldsymbol{U}} + \boldsymbol{\tau}^{-1}(\boldsymbol{U})\check{\boldsymbol{U}} = \check{P}[\mathbf{F} - \mathcal{L}(\boldsymbol{U},\boldsymbol{U}_h) - M(\boldsymbol{U})\partial_t \boldsymbol{U}_h],$$

where, for simplicity, we have assumed that the terms on the left hand side already belong to the space of subscales and thus their projection onto $\check{W}$ its equal to the terms themselves.

Different types of VMS methods arise when we provide distinct definitions of the projection operator $\check{P}$. When one considers the space of subscales as that of the residuals, i.e., one sets $\check{P} = I$ (the identity operator) when applied to the finite element residuals, the method which arises is termed Algebraic SubGrid-Scale (ASGS) [34]. Although this method is the simplest one, it is not really suitable for designing fractional step schemes. The ASGS approach combined with a segregation technique involves to compute the inverse of matrices with a wide stencil, which is usually computationally unaffordable. When the space of subscales $\check{W}$ is enforced to be L^2-orthogonal to the finite element space W_h, the method is termed Orthogonal SubGrid-Scale (OSGS or simply OSS). It corresponds to taking $\check{P} = P_h^{\perp} = I - P_h$ where P_h is the projection operator onto the finite element space without boundary conditions. This definition makes the subscales active in regions which cannot be resolved by the finite element mesh. Both of these methods are residual based by construction, and hence also consistent, being consistency understood in the finite element context, that is to say, the stabilization terms which modify the variational form of the problem vanish when the continuous solution is introduced.

6.3. Stabilized formulation applied to the isentropic Navier–Stokes problem

Once the general procedure has been described, let us apply these ideas to the isentropic compressible case. For reasons already discussed, we consider the OSGS technique. Let us depart from the following problem for the finite element scales (still continuous in time):

$$\langle \mathcal{D}_t(\boldsymbol{U}_h), \boldsymbol{V}_h \rangle + B(\boldsymbol{u}^*; \boldsymbol{U}_h, \boldsymbol{V}_h) + B_\Gamma(\boldsymbol{U}_h, \boldsymbol{V}_h) - \sum_{K\in\mathcal{T}_h} \left\langle \frac{1}{c^2\varrho}(\boldsymbol{u}^*\cdot\nabla)q_h + \nabla\cdot\boldsymbol{v}_h, \check{p} \right\rangle_K - \sum_{K\in\mathcal{T}_h} \left\langle \varrho(\boldsymbol{u}^*\cdot\nabla)\boldsymbol{v}_h + \mu\Delta\boldsymbol{v}_h + \frac{\mu}{3}\nabla(\nabla\cdot\boldsymbol{v}_h) + \nabla q_h, \check{\boldsymbol{u}} \right\rangle_K = L(\boldsymbol{V}_h),$$

for all test functions $\boldsymbol{V}_h$, where the symbols $\check{\boldsymbol{u}}$ and $\check{p}$ denote, respectively, the velocity and pressure subscales. For simplicity we will take the advection velocity to be $\boldsymbol{u}^* = \boldsymbol{u}_h$ (see e.g. [35] for the effect of taking $\boldsymbol{u}^* = \boldsymbol{u}_h + \check{\boldsymbol{u}}$). A simple calculation shows that the last two terms on the left hand side correspond to $\langle \check{\boldsymbol{U}}, \mathcal{L}^*(\boldsymbol{U}, \boldsymbol{V}_h)\rangle$ in (33). Likewise, the subgrid scales are computed as the solution of the following system:

$$\varrho\partial_t\check{\boldsymbol{u}} + \tau_1^{-1}\check{\boldsymbol{u}} = P_h^\perp\Big[\boldsymbol{f} - \varrho\partial_t\boldsymbol{u}_h - \varrho(\boldsymbol{u}^*\cdot\nabla)\boldsymbol{u}_h + \mu\Delta\boldsymbol{u}_h + \frac{\mu}{3}\nabla(\nabla\cdot\boldsymbol{u}_h) - \nabla p_h\Big], \tag{36}$$

$$\frac{1}{c^2\varrho}\partial_t\check{p} + \tau_2^{-1}\check{p} = P_h^\perp\left[-\frac{1}{c^2\varrho}\partial_t p_h - \frac{1}{c^2\varrho}(\boldsymbol{u}^*\cdot\nabla)p_h - \nabla\cdot\boldsymbol{u}_h\right], \tag{37}$$

where matrix $\boldsymbol{\tau}$ in (35) has been taken of the form $\boldsymbol{\tau} = \mathrm{diag}(\tau_1\boldsymbol{I}_d, \tau_2)$, $\boldsymbol{I}_d$ being the $d\times d$ identity matrix. Several remarks are now in order:

Remark 6.1. A simple approach is to neglect the time derivatives of the subscales in (36)-(37). In this situation, the subcales are named quasi-static in contrast to dynamic subscales, when they are considered to be time-dependent. Quasi-static subscales can be unstable in time for anisotropic space-time discretization (see [36–38] and references therein).

Remark 6.2. It is assumed that the orthogonal projections of the residual temporal terms cancels, i.e., $P_h^\perp[\varrho\partial_t\boldsymbol{u}_h] \approx 0$ and $P_h^\perp[\frac{1}{c^2\varrho}\partial_t p_h] \approx 0$. They would be exactly zero if both ϱ and c were equal to a constant, which is not the case for the isentropic problem. However, we consider as true that both variables are such that $\varrho\partial_t\boldsymbol{u}_h$ and $\frac{1}{c^2\varrho}\partial_t p_h$ already belong to the finite element spaces and hence its orthogonal projection onto $V_h^d \times Q_h$ vanishes. Additionally, we assume $P_h^\perp[\boldsymbol{f}] \approx 0$, which yields a weakly consistent method.

From the point of view of stability, not all the terms of the finite element residual in (36)-(37) aid to enhance the stability of the formulation. Therefore, some of them could be even neglected and a less costly method emerges. Precisely, it is this last idea the one that motivates the socalled term-by-term stabilization methods [22,39].

6.4. Term-by-term stabilization and monolithic formulation

The stabilized formulation we favor in this work is a term-by-term OSS approach, also referred as split OSS. Although this scheme is not completely residual-based, it has been proven that it has an optimal consistency error (see [40] for a formal discussion and numerical analysis on the Oseen equations). The key idea behind this method resides in neglecting the extra cross products among operators applied on both test and trial functions, which arise from the classical orthogonal stabilization. Let us rewrite (36)-(37) as follows,

$$\varrho\partial_t\check{\boldsymbol{u}} + \tau_1^{-1}\check{\boldsymbol{u}} = -P_h^\perp[\varrho(\boldsymbol{u}_h\cdot\nabla)\boldsymbol{u}_h] - P_h^\perp[\nabla p_h] + P_h^\perp[\mu\Delta\boldsymbol{u}_h] + P_h^\perp\Big[\frac{\mu}{3}\nabla(\nabla\cdot\boldsymbol{u}_h)\Big], \tag{38}$$

$$\frac{1}{c^2\varrho}\partial_t\check{p} + \tau_2^{-1}\check{p} = -P_h^\perp[\nabla\cdot\boldsymbol{u}_h] - P_h^\perp\left[\frac{1}{c^2\varrho}(\boldsymbol{u}_h\cdot\nabla)p_h\right]. \tag{39}$$

It is clear that omitting any of the projections in (38)-(39) would have a remarkable effect on the stability of the final formulation, yet this does not affect the general accuracy of the scheme. In order to provide stability and convergence on both convective terms, $P_h^\perp[-\varrho(\boldsymbol{u}_h\cdot\nabla)\boldsymbol{u}_h]$ and $P_h^\perp[-\frac{1}{c^2\varrho}(\boldsymbol{u}_h\cdot\nabla)p_h]$ are essential. In addition, control is also needed over the pressure gradient, $P_h^\perp[-\nabla p_h]$. Thus, we might neglect the viscous terms $P_h^\perp[\mu\Delta\boldsymbol{u}_h] + P_h^\perp\big[\frac{\mu}{3}\nabla(\nabla\cdot\boldsymbol{u}_h)\big]$. We also consider that both velocity and pressure subscales can be split in the form $\check{\boldsymbol{u}} = \check{\boldsymbol{u}}_1 + \check{\boldsymbol{u}}_2$ and $\check{p} = \check{p}_1 + \check{p}_2$, each component corresponding to the first and second terms in the right hand side of (38) and (39), so that the stabilization terms are independent (see [41]).

Taking all this into account, the term-by-term finite element formulation we propose in this work reads: find $\boldsymbol{U}_h \in L^2(0,T; V_h^d \times Q_h)$ such that,

$$\langle \mathcal{D}_t(\boldsymbol{U}_h), \boldsymbol{V}_h \rangle + B(\boldsymbol{u}_h; \boldsymbol{U}_h, \boldsymbol{V}_h) + B_\Gamma(\boldsymbol{U}_h, \boldsymbol{V}_h) - \sum_{K\in\mathcal{T}_h}\langle \varrho(\boldsymbol{u}_h\cdot\nabla)\boldsymbol{v}_h, \check{\boldsymbol{u}}_1\rangle_K - \sum_{K\in\mathcal{T}_h}\langle \nabla\cdot\boldsymbol{v}_h, \check{p}_1\rangle_K - \sum_{K\in\mathcal{T}_h}\langle \nabla q_h, \check{\boldsymbol{u}}_2\rangle_K - \sum_{K\in\mathcal{T}_h}\left\langle \frac{1}{c^2\varrho}(\boldsymbol{u}_h\cdot\nabla)q_h, \check{p}_2 \right\rangle_K = L(\boldsymbol{V}_h),$$

for all test functions $\boldsymbol{V}_h \in V_h^d \times Q_h$.

The stabilization parameters τ_1 and τ_2 defined over each element $K \in \mathcal{T}_h$ contribute to provide the stabilization for the weak forms of the momentum and mass conservation equations. Their definition is based on a Fourier analysis, which we will not discuss here (see [20]). They are computed as:

$$\tau_1 = \left[\mathcal{C}_1\frac{\mu}{h^2} + \mathcal{C}_2\varrho\frac{|\boldsymbol{u}_h|_K}{h}\right]^{-1} \quad ; \quad \tau_2 = \frac{h^2}{\mathcal{C}_1\tau_{1,K}},$$

where $|\boldsymbol{u}_h|_K$ is the mean Euclidean norm of the velocity in each element $K \in \mathcal{T}_h(\Omega)$. Note that their values are needed at each integration point. The algorithmic constants $\mathcal{C}_1$ and $\mathcal{C}_2$ depend on the polynomial order of the interpolation. For linear elements, it is commonly set $\mathcal{C}_1 = 4$ and $\mathcal{C}_2 = 2$. The four subscales $\check{\boldsymbol{u}}_1$, $\check{\boldsymbol{u}}_2$, $\check{p}_1$ and $\check{p}_2$ are computed from the solution of:

$$\begin{aligned}
\varrho\partial_t\check{\boldsymbol{u}}_1 + \tau_1^{-1}\check{\boldsymbol{u}}_1 &= -P_h^\perp[(\boldsymbol{u}_h\cdot\nabla)\boldsymbol{u}_h],\\
\frac{1}{c^2\varrho}\partial_t\check{p}_1 + \tau_2^{-1}\check{p}_1 &= -P_h^\perp[\nabla\cdot\boldsymbol{u}_h],\\
\varrho\partial_t\check{\boldsymbol{u}}_2 + \tau_1^{-1}\check{\boldsymbol{u}}_2 &= -P_h^\perp[\nabla p_h],\\
\frac{1}{c^2\varrho}\partial_t\check{p}_2 + \tau_2^{-1}\check{p}_2 &= -P_h^\perp\left[\frac{1}{c^2\varrho}(\boldsymbol{u}_h\cdot\nabla)p_h\right],
\end{aligned}$$

with zero initial condition for all of them. From this point, one can choose either to include the time derivatives of the subscales or to neglect them. For the sake of clarity in the exposition, let us

Algorithm 2 First and second order stabilized fractional step scheme for the isentropic problem, $k = 1, 2$.

1. Nonlinear problem to compute the intermediate velocity $\widetilde{\mathrm{U}}^{n+1}$using the pressure extrapolations:

   Set $\widetilde{\mathrm{U}}^{n+1,0} = \mathrm{U}^{n}$. For $i = 0, 1, 2, \ldots$ until convergence, compute $\widetilde{\mathrm{U}}^{n+1,i+1}$ from:

$$\mathrm{M}_{\boldsymbol{u}}\frac{\delta_k}{\delta t}\widetilde{\mathrm{U}}^{n+1,i+1} + \mathrm{K}_{\boldsymbol{u}}(\widetilde{\mathrm{U}}^{n+1,i})\widetilde{\mathrm{U}}^{n+1,i+1} + \mathrm{S}_{\boldsymbol{u}}(\widetilde{\mathrm{U}}^{n+1,i})\widetilde{\mathrm{U}}^{n+1,i+1} + \mathrm{M}_{\Gamma}\widetilde{\mathrm{U}}^{n+1,i+1} + \mathrm{K}_{\Gamma}\widetilde{\mathrm{U}}^{n+1,i+1} = \mathrm{F}^{n+1} + \mathrm{F}^{n+1}_{\Gamma,\boldsymbol{u}} - \mathrm{G}\widehat{\mathrm{P}}^{n+1}_{k-1} - \mathrm{G}_{\Gamma}\widehat{\mathrm{P}}^{n+1}_{k}$$

2. Compute the pressure P^{n+1} using the intermediate velocityfrom the previous step:

$$\mathrm{M}_{p}\frac{\delta_k}{\delta t}\mathrm{P}^{n+1} + \mathrm{K}_{p}(\widetilde{\mathrm{U}}^{n+1})\mathrm{P}^{n+1} + \mathrm{S}_{p}(\widetilde{\mathrm{U}}^{n+1})\mathrm{P}^{n+1} - \psi_k\delta t\mathrm{L}\mathrm{P}^{n+1} = \mathrm{F}^{n+1}_{\Gamma,p} - \mathrm{D}\widetilde{\mathrm{U}}^{n+1} - \mathrm{D}_{\Gamma}\widehat{\mathrm{U}}^{n+1}_{k} + \psi_k\delta t\mathrm{L}\widehat{\mathrm{P}}^{n+1}_{k-1}$$

3. Velocity correction to obtain the end-of-step velocity U^{n+1}:

$$\frac{1}{\psi_k\delta t}\mathrm{M}_{\boldsymbol{u}}\mathrm{U}^{n+1} + \mathrm{M}_{\Gamma}\mathrm{U}^{n+1} = \frac{1}{\psi_k\delta t}\mathrm{M}_{\boldsymbol{u}}\widetilde{\mathrm{U}}^{n+1} + \mathrm{M}_{\Gamma}\widetilde{\mathrm{U}}^{n+1} - \mathrm{G}(\mathrm{P}^{n+1} - \widehat{\mathrm{P}}^{n+1}_{k-1})$$

consider the steady behavior of subscales. Hence,

$$\check{\boldsymbol{u}}_1 = -\tau_1 P_h^{\perp}[(\boldsymbol{u}_h\cdot\nabla)\boldsymbol{u}_h], \quad \check{p}_1 = -\tau_2 P_h^{\perp}[\nabla\cdot\boldsymbol{u}_h],$$
$$\check{\boldsymbol{u}}_2 = -\tau_1 P_h^{\perp}[\nabla p_h], \quad \check{p}_2 = -\tau_2 P_h^{\perp}\left[\frac{1}{c^2\varrho}(\boldsymbol{u}_h\cdot\nabla)p_h\right].$$

The proposed method, which replaces the weak form (15) consists in finding $\boldsymbol{u}_h \in L^2(0,T;V_h^d\times Q_h)$, such that:

$$\langle\mathcal{D}_t(\boldsymbol{U}_h),\boldsymbol{V}_h\rangle + B(\boldsymbol{u}_h;\boldsymbol{U}_h,\boldsymbol{V}_h) + B_{\Gamma}(\boldsymbol{U}_h,\boldsymbol{V}_h) + B_1^{\perp}(\boldsymbol{u}_h;\boldsymbol{u}_h,\boldsymbol{v}_h) + B_2^{\perp}(\boldsymbol{u}_h;p_h,q_h) = L(\boldsymbol{V}_h), \tag{40}$$

for all $\boldsymbol{V}_h \in V_h^d\times Q_h$, satisfying the proper initial conditions and where,

$$B_1^{\perp}(\boldsymbol{u}_h;\boldsymbol{u}_h,\boldsymbol{v}_h) = \sum_{K\in\mathcal{T}_h}\left\langle\varrho(\boldsymbol{u}_h\cdot\nabla)\boldsymbol{v}_h,\tau_1P_h^{\perp}[\varrho(\boldsymbol{u}_h\cdot\nabla)\boldsymbol{u}_h]\right\rangle_K + \sum_{K\in\mathcal{T}_h}\left\langle\nabla\cdot\boldsymbol{v}_h,\tau_2P_h^{\perp}[\nabla\cdot\boldsymbol{u}_h]\right\rangle_K,$$

$$B_2^{\perp}(\boldsymbol{u}_h;p_h,q_h) = \sum_{K\in\mathcal{T}_h}\left\langle\frac{1}{c^2\varrho}(\boldsymbol{u}_h\cdot\nabla)q_h,\tau_2P_h^{\perp}\left[\frac{1}{c^2\varrho}(\boldsymbol{u}_h\cdot\nabla)p_h\right]\right\rangle_K + \sum_{K\in\mathcal{T}_h}\left\langle\nabla q_h,\tau_1P_h^{\perp}[\nabla p_h]\right\rangle_K.$$

The terms in $B_1^{\perp}(\boldsymbol{u}_h;\boldsymbol{u}_h,\boldsymbol{v}_h)$ and $B_2^{\perp}(\boldsymbol{u}_h;p_h,q_h)$ modify, respectively, the weak forms of the momentum and continuity equations. At the end we have obtained a stabilized formulation which adds the numerical diffusion in an efficient manner by means of completely symmetric terms.

6.5. Algebraic formulation and stabilized fractional step algorithm

The final variational formulation of the isentropic compressible problem was stated in (40). From there, the derivation of the matrix version is straightforward and the matrix system that needs to be solved at each time step has the same algebraic structure as (21)–(22) with the addition of two stabilization matrices, namely $\mathrm{S}_{\boldsymbol{u}}$ and S_p, which arise from the discretization of $B_1^{\perp}(\boldsymbol{u}_h;\boldsymbol{u}_h,\boldsymbol{v}_h)$ and $B_2^{\perp}(\boldsymbol{u}_h;p_h,q_h)$, respectively. Note that if the time dependency of subscales is not neglected, then the right hand side vectors of the system would also be modified in order to account for the contributions of the subscales from the previous time steps. With these observations in mind, the general procedure described in Section 5 is facilely extended to the stabilized algorithm.

We solve all possible nonlinearities considering a fixed-point approach, that is to say, taking the known values from the previous iteration. In Algorithm 2 we include the final scheme in its matrix form, where the superscript i denotes the nonlinear iteration counter. Note that the additional stabilization term in the system for the pressure, $\mathrm{S}_p(\widetilde{\mathrm{U}}^{n+1})\mathrm{P}^{n+1}$, does not need to be linearized considering any particular strategy since $\widetilde{\mathrm{U}}^{n+1}$ is already known by the time that P^{n+1} needs to be computed.

Finally, let us explain how we manage the orthogonal projections $P_h^{\perp}$. When compared to the raw Galerkin method, the matrices emerging from the orthogonal projection of the unknowns show a wide stencil. In order to avoid dealing with them, at the i-th iterion of the n-th time step we may approximate $P_h^{\perp}(g^{n,i}) \approx g^{n,i} - P_h(g^{n,i-1})$ or $P_h^{\perp}(g^{n,i}) \approx g^{n,i} - P_h(g^{n-1})$ for any generic function g. In other words, we perform the projection by means of known values from either the previous iteration or time step. Numerical tests reveal that both options are effective, the latter being chosen in the numerical examples included next.

7. Numerical results

In this section, some numerical examples are presented to show the performance of the proposed formulation. The first case we consider is a test with a manufactured solution in order to analyze the time discretization errors of the fractional step technique. After that, a 2D low-speed viscous flow over a cylinder at $\mathrm{Ma} = 0.0583$ is calculated. Later, we include a flow around a 3D NACA 0012 airfoil at $\mathrm{Ma} = 0.4$ and finally the noise radiated by the flow over a cavity at Ma=0.7 is discussed.

For all the numerical examples, the flow is considered as an ideal gas, with adiabatic coefficient $\gamma = 1.4$, molar mass $M = 0.02897$ kg/mol and temperature $\theta_0 = 293.15$ K. Hence, the speed of sound is $c_0 = 343.29$ m/s. In addition to this, the boundary formulation with the weak imposition of Dirichlet boundary conditions plus the NRBC is used, as explained in Section 3. Hence, a penalty parameter needs to be set to perform the simulation, β. In the case, this parameter behaves as $\beta = \beta_0(\mu/h + \varrho|\boldsymbol{u}_h|)$ for some constant β_0 and mesh size h, which will be fixed for each example. As previously discussed, the nonlinearities in the problem are solved via Picard's scheme. This leads to a monotonically decreasing relative error among consecutive iterations, ensuring the convergence of the method. A maximum of 20 iterations is set, and the numerical tolerance for the L^2 norm is 1×10^{-6}. In order to

solve the underlying systems of linear equations, we use the Biconjugate Gradients solver, `BiCGstab` [42], which is already implemented in the PETSc parallel solver library [43]. All units in the upcoming plots are in SI.

7.1. A test with analytical solution

Let us first perform a simple test whose main objective is to numerically check the time convergence of the fractional step schemes defined in Algorithm 2. For this purpose we use the so-called method of manufactured solutions. In this procedure, an exact analytical solution is defined a priori and later substituted into the continuum equations in order to obtain the associated forcing terms. Continuedly, these forcing terms are introduced as perturbations in the finite element computation. The time-dependent manufactured solutions are composed of smooth functions with no physical meaning. Dirichlet boundary conditions are prescribed weakly over the boundaries upon evaluation of the velocity analytical solution and the initial conditions arise from the prescribed functions evaluated at $t = 0$ over the whole computational domain.

The region we consider is the unit square, i.e. $\overline{\Omega} = [0, 1] \times [0, 1]$ and we assume the following manufactured fields,

$$\boldsymbol{u}(x_1, x_2, t) = g(t)[-\cos(x_1)\sin(x_2), \sin(x_1)\cos(x_2)] \tag{41}$$

$$p(x_1, x_2, t) = -\frac{1}{4}g^2(t)(\cos(2x_1) + \cos(2x_2)) \tag{42}$$

with $g(t) = \sin(2t)$, $t \in (0, 1)$ and x_1 and x_2 referring to the Cartesian axes. The values of air for density and viscosity at the bulk temperature have been used. A structured mesh of size $h = 0.05$ with bilinear elements has been employed to discretize the computational domain. Finally a constant $\beta_0 = 1000$ has been chosen to ensure a proper prescription of boundary conditions, thus avoiding excessive boundary errors.

The normalized error E has been computed in different norms: $\ell^\infty(L^2(\Omega))$ (maximum of the time sequence of spatial L^2-norms of the solution) and $\ell^2(H^1(\Omega))$ (ℓ^2-norm of the time sequence of spatial H^1-norms of the solution) for velocity, and $\ell^\infty(L^2(\Omega))$ for pressure. Fig. 2a shows the convergence plot for the fractional step algorithm using a BDF1 scheme in time and Fig. 2b for the case of second order, i.e., using BDF2. The reader can note that the proposed schemes in previou section shows the desired rate of convergence, and hence it is concluded that the extrapolations of the boundary terms explained in Section 5 do maintain the general temporal accuracy of the method. From the convergence plots it is also observed that the spatial error is not significant for the mesh size used.

7.2. Aeolian tones of low Mach viscous flow

The second numerical example we have considered for a proper assessment of the proposed formulation is the benchmark consisting in the aerodynamic sound radiated by an uniform flow past a cylinder, what is commonly referred as aeolian tones problem in the literaute (see e.g. [44,45]). In this example, the cylinder undergoes lift fluctuations in response to the vortex shedding generated at the lee of the cylinder, and such fluctuations generate the sound pressure pulses. The emitted sound is named aeolian tone.

The problem domain is $[0, L] \times [0, L]$ with $L = 200$ m, with the cylinder diameter $D = 0.3$ m and located at the center point of the square. The domain is big enough to describe the far field conditions far away from the cylinder. The prescription of boundary conditions is as follows: the flow is injected from the left boundary with constant horizontal velocity $U = 20$ m/s. Over both upper and lower walls the vertical component of the velocity is imposed to zero. These prescriptions are done weakly, using $\beta_0 = 10$. We have taken a dynamic viscosity coefficient of $\mu = 0.006$ kg/(m s) and density of $\varrho = 1$ kg/m^3 to initiate the computation. All this information leads to the following Reynolds and Mach numbers, $\mathrm{Re} = 1000$, $\mathrm{Ma} = 0.0583$, used by the benchmark solution.

In order to complete the simulation, we set a filtering frequency of 50 Hz to avoid reflections at the external boundaries. The unstructured mesh for the simulation is composed of nearly 500,000 P1 elements using equal interpolation for velocity and pressure thanks to the stabilized formulation above discussed. The mesh near the cylinder wall is of $3 \times 10^{-3} D$ in size, so as to capture the expected high gradients in that region. The time step size selected for the computation is $\delta t = 1 \times 10^{-3}$ s. It is important to note that the time step has to be small enough in order to be able to reproduce the aeroacoustic signal in an adequate manner. The second order BDF2 scheme has been used for the large scales time evolution, while a first order scheme has been used for the tracking of subscales. We recall here the necessity of letting the code run for several time steps prior to the application of the boundary formulation, in order to accumulate representative data for the computations. The initial condition for the simulation is provided by several time steps of an incompressible segregated solver.

In Fig. 3a–3 b we present the flow pressure contour for a certain time step of the vortex shedding cycle, qualitatively comparing the proposed fractional step scheme with its monolithic version (for the same mesh and time step size), already validated in [8]. It can be observed that the pressure pulses evolve radially from the cylinder area with time, yet they do not propagate normally to the flow direction since this case is based on an uniform flow. Additionally for this configuration of the flow, the classical oscillating wake after the cylinder is also developed (cf. Fig. 3c). Fig. 3d displays the pressure pulse along the positive x_2 axis for both for-

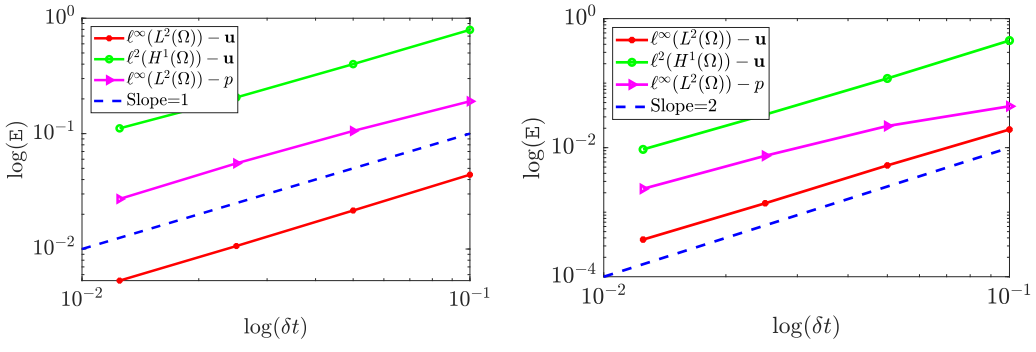

Fig. 2. Convergence test results for the proposed fractional step algorithm for the isentropic compressible Navier–Stokes problem: (a) BDF1 scheme, (b) BDF2 scheme.

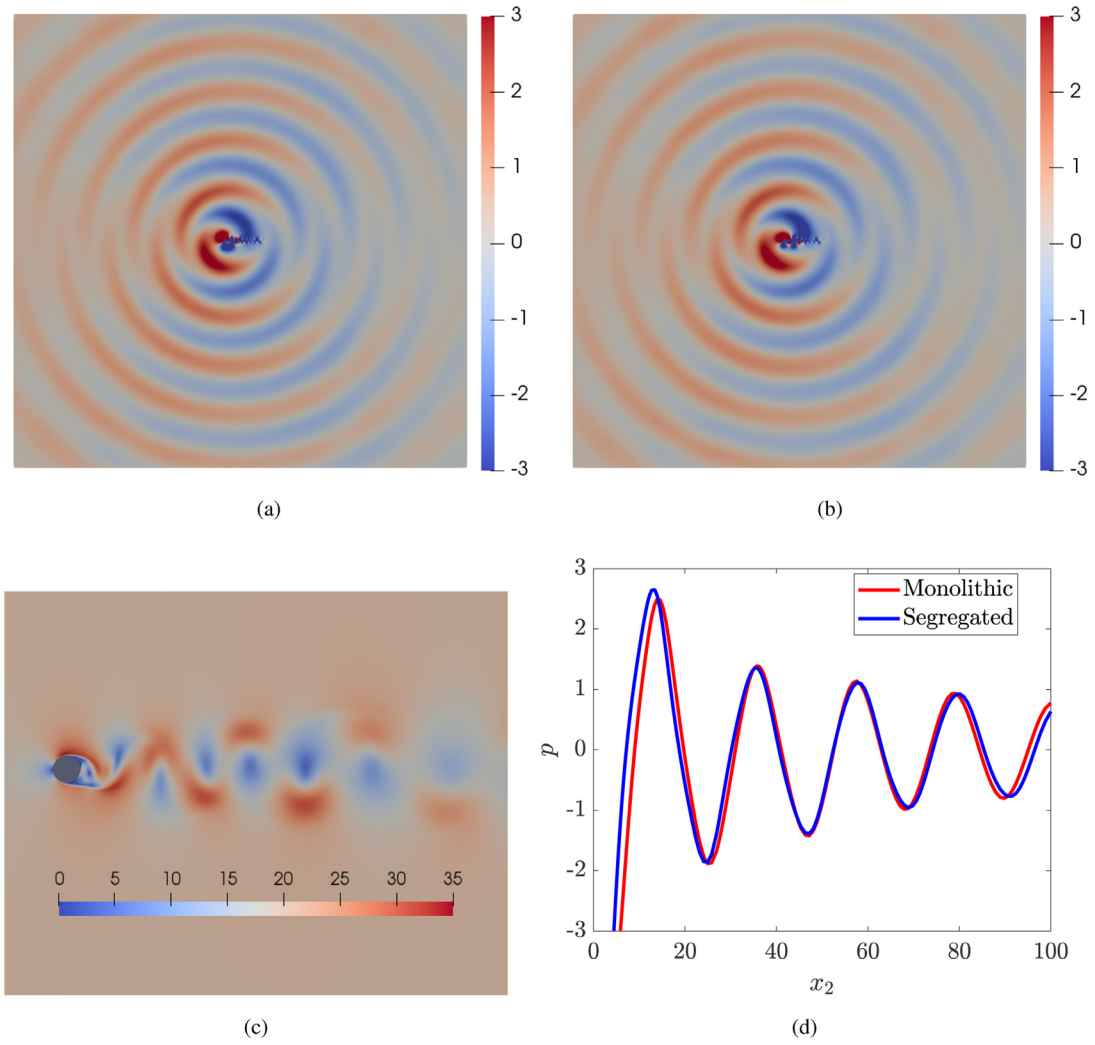

Fig. 3. Aeolian tones: (a) flow pressure contour for the segregated scheme, (b) pressure contour for the monolithic case, (c) velocity contour in the near field and (d) comparison of wave propagation along the x_2 direction.

mulations for the same time instant. The reader can notice that the acoustic wave propagation obtained with the segregation algorithm manages to reasonably reproduce the amplitude and frequency of the wave obtained with the monolithic reference scheme. Although some minor discrepancies might be noticed, the overall results are equivalent in a reasonable manner. The differences should come from the errors introduced by the fractional step approach and the approximate boundary condition.

As pointed out previously, the behavior of pressure waves once they reach the external artificial boundaries is a controversial situation in compressible solvers. The raw isentropic formulation would lead to the reflection of waves into the computational domain, but the compatible prescription for flow and acoustic variables adopted in this work allows the pressure pulses to abandon the domain in a smooth fashion. This fact demonstrates the satisfactory performance of the weak imposition of Dirichlet boundary conditions combined with a segregation technique and, similarly, it exposes the ability of the non-reflecting boundary conditions to attenuate the propagated sound waves.

In order to further asses the suitability of the fractional step approach so as to replace its monolithic counterpart (taken as reference), we perform a comparison on both non-dimensional lift C_L and drag C_D coefficients of the cylinder. In order to illustrate this point, the time histories of these coefficients are included in Fig. 4a and b. Both exhibit the expected sinusoidal behavior, with minimal deviation between the two formulations, as a result of the segregation error. We also take these historical values to the frequency domain via a Fourier transform algorithm, and the results are shown in Figs. 4c and d. For the case of the lift coefficient and the monolithic scheme, it has an amplitude of 1.363 and oscillates at the vortex shedding frequency of 15.625 Hz (St $= 0.234$). These values have a remarkable agreement with the ones reported in [45], where the problem is solved using a convected Helmholtz equation (see Section 4.2 in that publication). When the solution is obtained with the segregated approach, C_L has an amplitude of 1.335 and shows a frequency of 15.435 Hz (St $= 0.231$). In addition to this, the drag coefficient displays an amplitude of 0.181 for the monolithic solution and 0.169 for the fractional counterpart. In terms of frequency, C_D oscillates at 31.251 Hz for the monolithic (which is precisely twice the vortex shedding frequency) and at 31.105 Hz for the segregated algorithm, what translates into a relative error of $\sim 0.5\%$ with respect to the reference solution. These values are collected in Table 1 down below.

The computational savings that segregation techniques offer when compared to monolithic schemes are undoubted. The linear systems to be solved in fractional step methods are smaller and

Table 1
Comparison of frequency and amplitude values for the non-dimensional lift and drag coefficients when the solution of the problem is computed with the monolithic or fractional step algorithms.

	Monolithic		Fractional step	
	Amplitude [-]	Frequency [Hz]	Amplitude [-]	Frequency [Hz]
C_L	1.363	15.625	1.335	15.435
C_D	0.181	31.265	0.169	31.105

better conditioned, and usually each unknown requires a distinct number of iterations to solve its corresponding linear system. Although in this example we have used the same solver for all subsystems arising in the segregation method, specific solving techniques could be exploited in order to improve the performance of fractional step schemes even further. For the problem in hand, it was obtained that the CPU time of the fractional step algorithm over the CPU time of the monolithic case was 0.39. In other words, the computational savings go up to 60%.

In view of the information provided by previous quantitative comparisons, we can conclude that the fractional step approach is an effective alternative to the classical monolithic technique.

7.3. Aerodynamic sound generated by the flow past an airfoil

The next example consists in the uniform flow over a NACA 0012 airfoil with an angle of attack of 5°, which will be used for an extra qualitative validation of the formulation developed in this work. Similarly as in the cylinder example, the vortex shedding phenomena originates the pressure pulses which emanate from the airfoil surface. This same geometry has been solved in [46] by means of a compressible LES model for the flow scales plus an acoustic analogy to compute the acoustic component. It is not our goal in this simulation to investigate the performance of the isentropic solver in specific mesh typologies or to replicate the details of a particular problem and conditions, but to examine the propagation of the acoustic scales and the applicability of the solver to reproduce flow patterns at Ma= 0.4. Additionally, this example is intended to show the capability of the implementation to handle 3D configurations avoiding spurious reflections at the external contours.

The configuration of the domain is the box $[0, L] \times [0, H] \times [0, W]$ with $L = 15$ m, $H = 10$ m and $W = 1$ m. The airfoil has its trailing edge located at point (5,5) and its chord line is of $d = 0.1524$ m in length. The prescription of the boundary conditions is essentially the same as for the cylinder problem in the previous subsection,

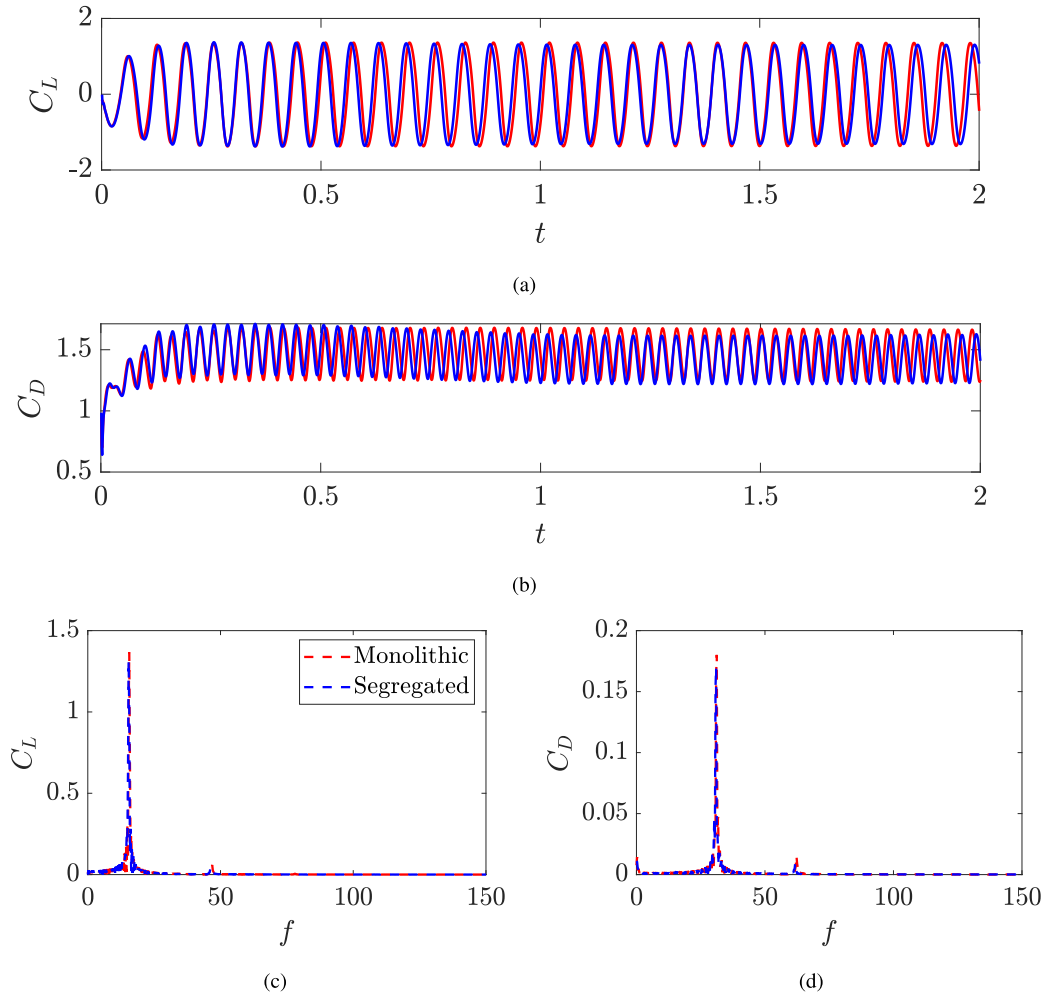

Fig. 4. Aeolian tones: (a) time evolution of non-dimensional lift coefficient, (b) time evolution of non-dimensional drag coefficient, (c) non-dimensional lift coefficient spectrum (d) non-dimensional drag coefficient spectrum. In all figures red and blue colors refer to monolithic and fractional step results, respectively. (For interpretation of the references to color in this figure legend, the reader is referred to the web version of this article.)

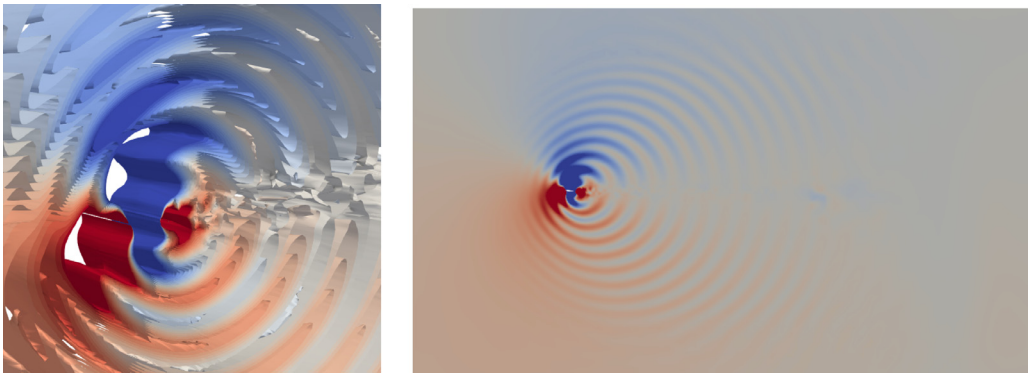

(a) (b)

Fig. 5. Flow past an airfoil: (a) close-up view of the pressure isosurfaces around the airfoil, (b) pressure contour plot (scale between $\mp$ 150 Pa) over the plane $x_3 = 0$, free of spurious reflections on the boundary.

yet over the walls on the x_3 direction we assign periodic boundary conditions. The incident horizontal velocity in the left surface is chosen to be $U = 140$ m/s, and we take $\mu = 2.56 \times 10^{-3}$ kg/(m s) and $\varrho = 1.2$ kg/m^3. Therefore the Reynolds and Mach numbers are Re $\approx 10,000$ and Ma $= 0.4$. The cutoff frequency for this problem is set to 1, 000 Hz. For the simulation, the domain is discretized with a semi-structured mesh which entails about 800,000 tetrahedral elements. The case has been run up to $T = 0.1$ s with a time step size of $\delta t = 1 \times 10^{-5}$ s. The coefficient for the weak imposition of Dirichlet boundary conditions has been taken as $\beta_0 = 3$. A BDF2 scheme has been used for the large scales evolution, and a first order scheme has been used for the tracking of subscales.

In Fig. 5 we include the pressure wave propagation towards the far field. It is observed that pressure waves evolve from the airfoil area, and eventually reach the artificial exterior boundaries. Although in the nearest region around the airfoil the propagation is not clearly visible since it is small compared to the aerodynamic scale (precisely one of the downsides of DNC), it eventually evolves comparably as in [46]. Again, the most important feature is that the solution is not polluted by spurious pressure reflections. Our fractional step implementation is capable of prescribing the scale separation avoiding reflections in a reasonable manner, since it accounts for smooth variations of the mean flow variables which do not interfere with the acoustic field evolution.

Similarly, we compared the computational times of the segregation scheme with respect to the monolithic counterpart. For this 3D computation, the ratio of CPU times turns out to be 0.25, what reveals even a further reduction in comparison with the previous 2D problem.

7.4. Noise radiated by the flow past an open cavity

As a final numerical example, the simulation of the noise radiated by a 2D flow past an open cavity is performed in order to further investigate the aeroacoustic feedback of the formulation. The problem setting consists in an infinitely long rectangular cavity of aspect ratio 2, with depth $D = 0.00254$ m and length $L = 2D$. The accurate simulation of the acoustic radiation from the cavity relies on an adequate definition of the boundaries. Hence, the computational domain extends over $H = 25D$ vertically and $W = 50D$ horizontally, meaning that both upstream and downstream walls are sufficiently far away from the cavity itself in order to avoid any possible self-forcing and to allow a proper impinging of the propagated sound waves, see Fig. 6a. This is a challenging problem, where acoustics and flow dynamics are highly coupled. Essentially, periodic vortices are formed just downstream the leading edge of the cavity, and when they impinge the trailing edge, pressure pulses are generated which start propagating upstream.

Non slip boundary conditions are prescribed on the cavity walls and the flow is injected at the left-most side with uniform velocity $U = 245$ m/s. The right-most side is left free and over the higher wall the vertical component of the velocity is prescribed to zero. Additional parameters for the simulation are chosen as follows: $\varrho = 1.16$ kg/m^3, $\mu = 1.76 \times 10^{-5}$ kg/(m/s), $\beta_0 = 25$, $\delta t = 5 \times 10^{-7}$, and the filtering frequency is 5,000 Hz. Hence, we obtain Ma $= 0.7$ and Re $= 41,000$ (based on cavity depth), conditions that have been studied by several authors in the literature [47–49]. An unstructured mesh with nearly 275,000 triangular elements is used for the computations.

Let us start by assessing the far-field results. We monitored the pressure history at point P with coordinates $x_1 = -0.04D$ and $x_2 = 2D$ which is located at the beginning at the acoustic region outside the cavity. Fig. 6b shows the corresponding sound pressure level spectrum versus the Strouhal number, St $= fL/U$. The principal peak is located at St $= 0.64$ whereas in [49] (where a DNS of the compressible flow equations is performed and taken as reference here) it is located at St $= 0.66$, what induces a small error. A maximum of 158 dB was obtained, which agrees with the values shown in that publication. Most important, the slope of the cascade that appears at higher Strouhal numbers is similar, what validates the formulation in terms of energy transfer.

Likewise, the propagation of acoustic waves can be visualized and compared in Fig. 6c and d. Pressure contours obtained in the present simulation, in contrast to the ones from Gloerfelt et al. [49] are depicted. Visual comparisons of the radiated pressure field coincide reasonably. The reader should also note that the computational domain used for the simulation does not affect the solution as it allows to damp completely the reflection of the sound waves at the artificial walls. The aforementioned agreement cannot be achieved without the use of non-reflecting conditions (or any similar damping technique).

With regard to the near field results, Fig. 6e and f present the vorticity and pressure fields for a given time instant once the fluctuating mechanism is established. In Fig. 6e one can observe different vortical structures. One of them inside the cavity, as the interaction between flow and acoustics causes a highly chaotic behavior in this region. Another vortex can be seen just above the trailing edge. As the vortex first hits this edge, it spills over the corner and, eventually, it is convected downstream, increasing the thickness of the reattached boundary layer. Fig. 6f is the corresponding pressure field. A recirculation zone is located in the second half of the cavity, which is mainly associated with the low pressure region in the plot (in blue). In addition, a subsequent high-low pressure

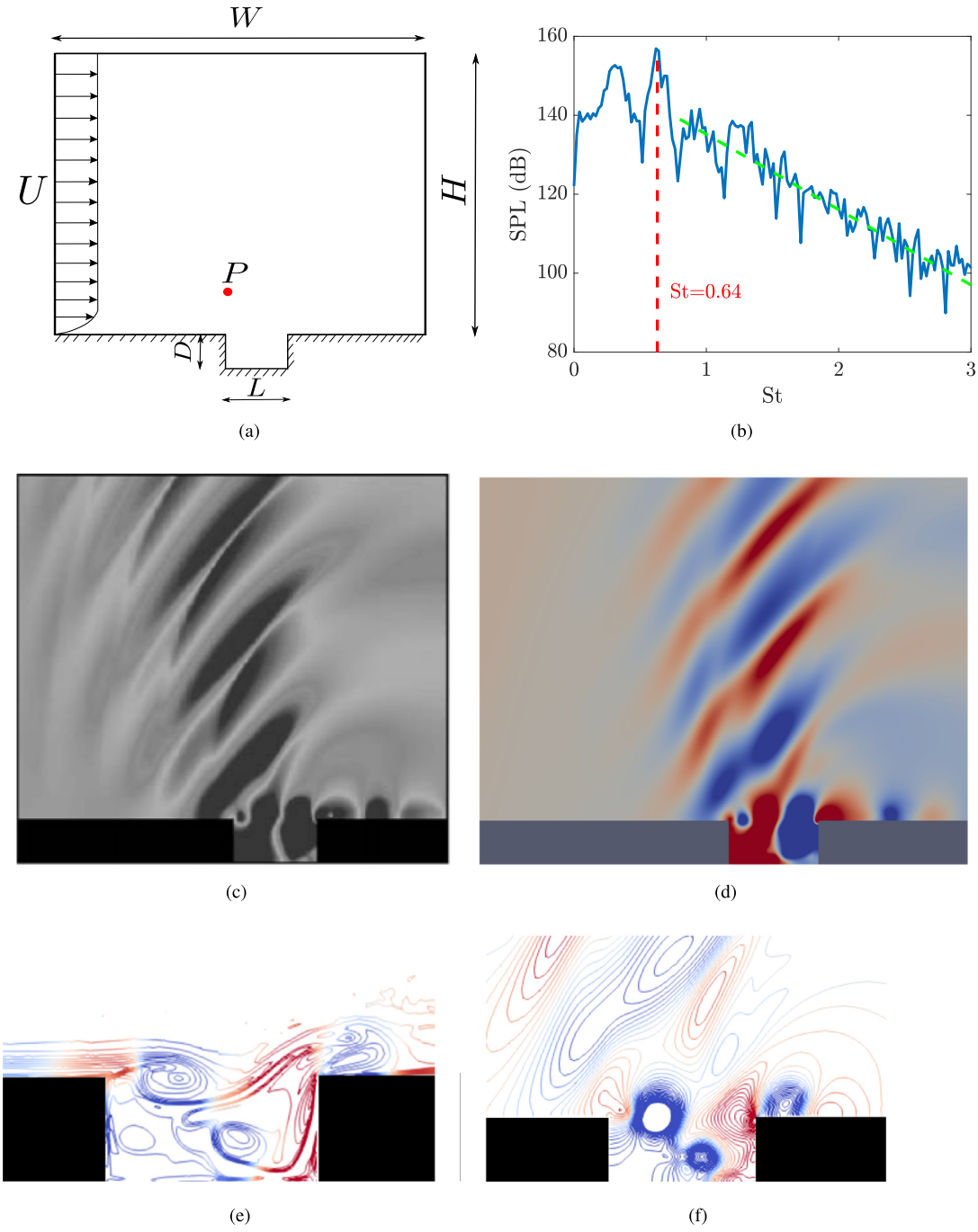

Fig. 6. Flow past a cavity: (a) cavity flow problem setting, (b) spectrum of pressure fluctuations versus the Strouhal number at the beginning of the acoustic region, (c) DNS reference pressure field [49], (d) calculated pressure field using the second order fractional step approach (scale between ∓ 3000 Pa), (e) vorticity contours and (f) pressure contours for a given time instant within the main oscillation. Fifteen contours between $\omega_{x_3} D/U = -10.5$ and 1.35 for vorticity and twenty five contours between ∓ 10000 Pa for pressure are used. (For interpretation of the references to color in text, the reader is referred to the web version of this article.)

structure outside the cavity can be observed, which is propagating towards the far field. This sequence can be directly compared to the ones presented in [49] (see Section 2 in that publication), so we conclude that the present implementation manages to reproduce the same flow patterns (same scaling is used for the comparison).

8. Conclusions

In this article, a methodology up to second order in time to solve the isentropic compressible Navier–Stokes equations in a segregated manner has been presented. The formulation is constructed using the extrapolation concept at the pure algebraic level. From the numerical point of view, the fractional step approach has been combined with other ingredients, such as the split-orthogonal and dynamic definition of subscales, the weak imposition of Dirichlet boundary conditions via extrapolations of boundary terms and the application of non-reflecting boundary conditions, a major issue in compressible solvers.

The accuracy of the resulting schemes has been tested numerically using the method of manufactured solutions, obtaining optimal convergence rates for smooth enough solutions. Additionally,

the implementation managed to reproduce the aeolian tones radiated by a flow past a cylinder, a convective simulation of a 3D airfoil geometry, and the problem of flow past a cavity at $M = 0.7$. All these examples completely cover the subsonic range and highlight the satisfactory performance of the proposed prescription of boundary conditions, combining Nitsche's method and a Sommerfeld-like non-reflecting condition in a segregated approach. The inclusion of the latter is crucial in this problem, in which reflections at the boundaries develop oscillations and instabilities that end up affecting the simulation results if a standard methodology is used. In addition to this, an important reduction in the CPU time with respect to the monolithic case has been verified.

The low implementation requirements when departing from a Navier–Stokes (incompressible) solver, added to the computational savings of the segregated approach, make this algorithm appealing for aeroacoustic problems within the subsonic regime, where shocks and heat transfer can be neglected.

Declaration of Competing Interest

The authors declare that they have no known competing financial interests or personal relationships that could have appeared to influence the work reported in this paper.

Acknowledgments

Samuel Parada gratefully acknowledges the support received from the Agència de Gestió d'Ajuts Universitaris i de Recerca through the predoctoral FI grant 2019-FI-B-00607. Joan Baiges gratefully acknowledges the support of the Spanish Government through the Ramón y Cajal grant RYC-2015-17367. Ramon Codina gratefully acknowledges the support received from the ICREA Acadèmia Research Program of the Catalan Government. This work was partially funded through the TOP-FSI: RTI2018-098276-B-I00 project of the Spanish Government.

References

[1] Bailly C, Bogey C, Marsden O. Progress in direct noise computation. Noise Not 2010;9(3):31–48. doi:10.1260/1475-472X.9.1-2.123.
[2] Bayona C, Baiges J, Codina R. Variational multi-scale finite element solution of the compressible Navier–Stokes equations. Int J Numer Methods Heat Fluid Flow 2015;26:1240–71. doi:10.1108/HFF-11-2015-0483.
[3] Lighthill MJ. On sound generated aerodynamically I. General theory. Proc R Soc 1952;211(1107):564–87. doi:10.1098/rspa.1952.0060.
[4] Hardin J, Pope D. An acoustic/viscous splitting technique for computational aeroacoustics. Theor Comput Fluid Dyn 1994;6(5–6):323–40. doi:10.1007/BF00311844.
[5] Shen WZ, Sørensen JN. Aeroacoustic modelling of low-speed flows. Theor Comput Fluid Dyn 1999;13(4):271–89. doi:10.1007/s001620050118.
[6] Shen WZ, Zhu W, Sørensen JN. Aeroacoustic computations for turbulent airfoil flows. Am Inst Aeronaut Astronaut 2009;47(6):1518–27. doi:10.2514/1.40399.
[7] Shen WZ, Michelsen JA, Sørensen JN. A collocated grid finite volume method for aeroacoustic computations of low-speed flows. J Comput Phys 2004;196(1):348–66. doi:10.1016/j.jcp.2003.11.006.
[8] Pont A, Codina R, Baiges J, Guasch O. Unified solver for fluid dynamics and aeroacoustics in isentropic gas flows. J Comput Phys 2018;363:11–29. doi:10.1016/j.jcp.2018.02.029.
[9] Chorin AJ. A numerical method for solving incompressible viscous problems. J Comput Phys 1967;2:12–26. doi:10.1006/jcph.1997.5716.
[10] Teman R. Sur l'approximation de la solution des equations de Navier–Stokes par la méthode des pas fractionaires (I). Arch Rat Mech Anal 1969;32:135–53. doi:10.1007/BF00247678.
[11] Badia S, Codina R. Algebraic pressure segregation methods for the incompressible Navier–Stokes equations. Arch Comput Methods Eng 2007;15(3):1–52. doi:10.1007/s11831-008-9020-3.
[12] Guermond J, Minev P, JShen. An overview of projection methods for incompressible flows. Comput Methods Appl Mech Eng 2006;195:6011–45. doi:10.1016/j.cma.2005.10.010.
[13] Codina R. Pressure stability in fractional step finite element methods for incompressible flows. J Comput Phys 2001a;170:112–40. doi:10.1006/jcph.2001.6725.
[14] Brooks A, Hughes T. Streamline upwind / Petrov–Galerkin formulations for convection dominated flows with particular emphasis on the incompressible Navier–Stokes equation. Comput Methods Appl Mech Eng 1982;32:199–259.
[15] Hughes T, Franca L, Hulbert G. A new finite element formulation for computational fluid dynamics: VIII. The Galerkin/Least–Squares method for advective–diffusive equations. Comput Methods Appl Mech Eng 1989;73:173–89.
[16] Donea J. A Taylor–Galerkin method for convection transport problems. Int J Numer Methods Eng 1984;20:101–19.
[17] Hughes T, Feijóo G, Mazzei L, Quincy J. The variational multiscale method–a paradigm for computational mechanics. Comput Methods Appl Mech Eng 1998;166:3–24.
[18] Hughes T. Multiscale phenomena: Green's function, the Dirichlet–to–Neumann formulation, subgrid scale models, bubbles and the origins of stabilized formulations. Comput Methods Appl Mech Eng 1995;127:387–401.
[19] Hughes T, Scovazzi G, Franca L. Multiscale and stabilized methods. Encyclopedia of Computational Mechanics. Wiley; 2017. doi:10.1002/9781119176817.ecm2051.
[20] Codina R. Stabilized finite element approximation of transient incompressible flows using orthogonal subscales. Comput Methods Appl Mech Eng 2002;191:4295–321. doi:10.1016/S0045-7825(02)00337-7.
[21] Castillo E, Codina R. Stabilized stress-velocity-pressure finite element formulations of the Navier-Stokes problem for fluids with non-linear viscosity. Comput Methods Appl Mech Eng 2014;279:554–78. doi:10.1016/j.cma.2014.07.003.
[22] Castillo E, Codina R. Finite element approximation of the viscoelastic flow problem: a non-residual based stabilized formulation. Comput Fluids 2017;142:72–8. doi:10.1016/j.compfluid.2016.07.012.
[23] Colonius T, Lele SK, Moin P. Boundary conditions for direct computation of aerodynamic sound generation. Am Inst Aeronaut Astronaut 1993;31(9):1574–82. doi:10.2514/3.11817.
[24] Fosso P, Deniau H, Lamarque N, Poinsot T. Comparison of outflow boundary conditions for subsonic aeroacoustic simulations. Int J Numer Methods Fluids 2012;68(10):1207–33. doi:10.1002/fld.2597.
[25] Granet V, Vermorel O, Léonard T, Gicquel I, Poinsot T. Comparison of non-reflecting outlet boundary conditions for compressible solver on unstructured grids. Am Inst Aeronaut Astronaut 2010;48(10):2348–64. doi:10.2514/1.J050391.
[26] Codina R, Baiges J. Weak imposition of essential boundary conditions in the finite element approximation of elliptic problems with non-matching meshes. Int J Numer Methods Eng 2015;104(7):624–54. doi:10.1002/nme.4815.
[27] Espinoza H, Codina R, Badia S. A Sommerfeld non-reflecting boundary condition for the wave equation in mixed form. Comput Methods Appl Mech Eng 2014;276:122–48. doi:10.1016/j.cma.2014.03.015.
[28] Oosthuizen P, Carscallen W. Introduction to Compressible Fluid Flow. CRC Press; 2013.
[29] Avila M, Principe J, Codina R. A finite element dynamical nonlinear subscale approximation for the low Mach number flow equations. J Comput Phys 2011;230:7988–8009. doi:10.1016/j.jcp.2011.06.032.
[30] Juntunen M, Stenbeg R. Nitche's method for general boundary conditions. Math Comput 2009;78(267):1353–74. doi:10.1090/s0025-5718-08-02183-2.
[31] Castillo E, Codina R. First, second and third order fractional step methods for the three-field viscoelastic flow problem. J Comput Phys 2015;296:113–37. doi:10.1016/j.jcp.2015.04.027.
[32] Codina R, Folch A. A stabilized finite element predictor–corrector scheme for the incompressible Navier–Stokes equations using a nodal–based implementation. Int J Numer Methods Fluids 2004;44:483–503. doi:10.1002/fld.648.
[33] Codina R, Badia S, Baiges J, Príncipe J. Variational multiscale methods in computational fluid dynamics. Encyclopedia of Computational Mechanics, Second Edition; 2018. p. 1–28. doi:10.1002/9781119176817.ecm2117.
[34] Codina R. A stabilized finite element method for generalized stationary incompressible flows. Comput Methods Appl Mech Eng 2001b;190(20):2681–706. doi:10.1016/S0045-7825(00)00260-7.
[35] Colomés O, Badia S, Codina R, Principe J. Assessment of variational mulstiscale methods from the large eddy simulation of turbulent incompressible flows. Comput Methods Appl Mech Eng 2015;285:32–63. doi:10.1016/j.cma.2014.10.041.
[36] Badia S, Codina R. On a multiscale approach to the transient Stokes problem: dynamic subscales and anisotropic space–time discretization. Appl Math Comput 2009;207(2):415–33. doi:10.1016/j.amc.2008.10.059.
[37] Bochev P, Gunzburger M, Lehoucq R. On stabilized finite element methods for the Stokes problem in the small time step limit. Int J Numer Methods Fluids 2007;53(4):573–97. doi:10.1002/fld.1295.
[38] Codina R, Principe J, Guasch O, Badia S. Time dependent subscales in the stabilized finite element approximation of incompressible flow problem,. Comput Methods Appl Mech Eng 2007;196(21):2413–30. doi:10.1016/j.cma.2007.01.002.
[39] Rebollo TC. A term by term stabilization algorithm for finite element solution of incompressible flow problems. Numer Math 1998;79:283–319. doi:10.1007/s002110050341.
[40] Codina R. Analysis of a stabilized finite element approximation of the Oseen equations using orthogonal subscales. Appl Numer Math 2008;58:264–83. doi:10.1016/j.apnum.2006.11.011.
[41] Castillo E, Codina R. Dynamic term-by-term stabilized finite element formulation using orthogonal subgrid-scales for the incompressible Navier-Stokes problem. Comput Methods Appl Mech Eng 2019;349:701–21. doi:10.1016/j.cma.2019.02.041.
[42] der Vorst HAV. Bi-CGSTAB: a fast and smoothly converging variant of Bi-CG for the solution of nonsymmetric linear systems. SIAM J Sci Stat Comput 1992;13(2):631–44. doi:10.1137/0913035.
[43] Balay S, Abhyankar S, Adams MF, Brown J, Brune P, Buschelman K, et al. PETSc Web page; 2015. http://www.mcs.anl.gov/petsc

[44] Guasch O, Codina R. Computational aeroacoustics of viscous low speed flows using subgrid scale finite element methods. J Comput Acoust 2009;17(3):309–30. doi:10.1142/S0218396X09003975.
[45] Guasch O, Codina R. An algebraic subgrid scale finite element method for the convected Helmholtz equation in two dimensions with applications in aeroacoustics.. Comput Methods Appl Mech Eng 2007;196:4672–89. doi:10.1016/j.cma.2007.06.001.
[46] Wolf WR, Lele SK. Trailing edge noise predictions using compressible LES and acoustic analogy. Am Inst Aeronaut Astronaut 2012;50(11):2423–34. doi:10.2514/6.2011-2784.
[47] Rowley CW, Colonious T, Basu AJ. On self-sustained oscillations in two-dimensional compressible flow over rectangular cavities. J Fluid Mech 2002;455:315–46. doi:10.1017/S0022112001007534.
[48] Bres GA, Colonious T. Three–dimensional instabilities in compressible flow over open cavities. J Fluid Mech 2008;599:309–39. doi:10.1017/S0022112007009925.
[49] Gloerfelt X, Bailly C, Juvé D. Direct computation of the noise radiated by a subsonic cavity flow and application of integral methods. J Sound Vib 2003;266:119–46. doi:10.1016/S0022-460X(02)01531-6.